Department of Construction Sciences
Solid Mechanics

ISRN LUTFD2/TFHF-16/5209-SE(1-55)

Evaluation of Material Models to Predict Material Failure in LS-DYNA

Master's Dissertation by

Hjalmar Sandberg
Oscar Rydholm

Supervisors:
Johan Hektor, Div. of Solid Mech. LTH
Niclas Brännberg, CEVT AB

Examiner:
Matti Ristinmaa, Div. of Solid Mech. LTH

Printed by Media-Tryck AB, Lund, Sweden
For information, address:
Division of Solid Mechanics, Lund University, Box 118, SE-221 00 Lund, Sweden
Webpage: www.solid.lth.se

Abstract

Computer simulation of car crashes is an important tool in the car development process. With increased awareness of the environment, it is important that the excess of material usage for the car is minimized. The effect of the material reduction must not compromise the safety of the passengers. It is possible to use computer simulations for the reduced structure at a certain loading to see how the crashworthiness is affected. To be able to rely on the simulated result, it is necessary to have a material model that predicts the material behaviour accurately. CEVT is currently using an advanced material model called *MF GenYld+CrachFEM*[1]. The main drawbacks of this model are that it affect the simulation time in a high extent and it also requires an additional license cost.

The objective of the thesis is to implement a new material model and compare it to the current one. The material model that is considered is implemented within *LS-DYNA* and works as a combination of an elasto-plastic model called *MAT_024 and a failure model called *GISSMO*. The implementation requires the user to define a set of material parameters. To obtain these a characterization of the material is needed and since no experimental data is available for this thesis, this is done by simulated material tests where the material behaviour is modelled with MF GenYld+CrachFEM.

The two material models are compared during two complex load cases, one depicting a B-pillar[2] and one depicting a rear bumper crash. The two material models prove to have similar results, but the simulation with *MAT_024 and GISSMO reduce the simulation time extensively.

[1]The material model MF GenYld+CrachFEM is often referred to as just CrachFEM.

[2]Pillar located between the front- and the back door of a car.

Acknowledgement

The Master Thesis was carried out at CEVT in Gothenburg in cooperation with the Division of Solid Mechanics at Lund University. It was initiated in January 2016 and completed in June 2016.

Firstly, we would like to thank our supervisor at CEVT, Niclas Brännberg, for his patience and valuable discussions during the process. Secondly, we would like to give a special thanks to our supervisor at LTH, Johan Hektor, for his feedback and valuable support during the project. We would like to thank our colleagues at CEVT for making our stay pleasant. Finally, an extra thanks to Hans Merkle at CEVT and Mikael Schill at DYNAmore for helping us with theoretical and practical issues during the thesis.

Lund, June 2016
Oscar Rydholm and Hjalmar Sandberg

Contents

1 Introduction

1.1 China Euro Vehicle Technology AB (CEVT)

CEVT was founded in mid 2013 as a R&D center for the platform[3] of the C-segment[4] cars of Geely Group. CEVT has expanded from nine people to approximately 1500 at present time. Nowadays, the company is active as a subcontractor to Volvo Cars and Geely, where they still are working with the car platform and can also offer expertise with complete vehicle design. CEVTs offices are located in Gothenburg, Sweden and Hangzhou, China.

1.2 Background

Due to the global trend to reduce CO_2 emissions from vehicles, focus is pointed at decreasing the weight of the car. A demanding issue is to decrease the weight and still let the crashworthiness be remained. One way of examining the opportunities of this is to simulate the car's behaviour during a crash. Thereby, it is possible to estimate how the changes in structure affect the crashworthiness. However, to be able to use the simulated results as guidance, there are some factors that needs to be considered. The first step to make the simulation reliable, is to model the material behaviour accurately. Andrade, Feucht and Haufe [1] have flagged for another factor, there is an information gap between the forming process and crash analysis where important data is lost between the different development stages. An interest of closing the gap has arisen, since the forming operations may affect the crashworthiness of the produced parts. Another trend that Effelsberg et al. [7] claim, is that the new material models try to predict the actual failure behaviour, instead of just describing the initiation of material failure which have been the case earlier.

To be able to consider material failure in simulations, CEVT is currently using the proprietary material models from *Crachfem* by *Matfem*. These material models, which are based on an extensive set of material tests, can handle a number of different material models. Unfortunately, the simulation configuration for Crachfem is encrypted, which means that the input parameters are hidden and the whole model may be viewed as a black box.

The thesis project is of interest for CEVT since there are a few other drawbacks of CrachFEM. Firstly, the material model itself takes a substantial amount of time to process, and hence, it is slowing down the simulations. Secondly, the additional license cost for CrachFEM is high.

[3] A car platform is the under body of the car and the device that everything is attached to.

[4] The C-segment is a car classification that is done with respect to the car's size. It includes cars like Volkswagen Golf and Ford Focus.

1.3 Objective

This thesis shall evaluate a material failure model called GISSMO, General Incremental Stress-State dependent Damage Model, [13] and compare it with CrachFEM. The implementation of GISSMO require characteristic properties for the material used. To obtain these properties, a variety of material tests have to be performed. This project does not cover physical material tests and no experimental data are available. Thus, the input parameters for the material model will be generated from numerical simulations, where CrachFEM is used to model the material failure. To ensure that the characterization is done correctly, the thesis starts with a literature study. The study involves how to perform material tests, the theory behind the different material models and learning about the software that will be used. The specimens to the material testing have to be designed, meshed and applied with boundary conditions. This will be done in the software ANSA [17]. The simulations of the material tests will be performed in LS-DYNA [13], which is a solver that is widely used to perform finite element calculations in the automotive industry. These simulations will provide the fundamental material properties needed to implement GISSMO. Before the properties can be implemented, they need to be calibrated through reversed engineering with help of an optimization tool. This project will use a software called LS-OPT [4] to perform the optimization. When the new material model is implemented, it is to be compared with CrachFEM. The comparison will be done with two different complex load cases. The first load case is of a simplified B-pillar. This test will primarily measure the difference in simulation time between the models and secondarily notice tendencies of the material's failure behaviour. During the second load case, the loading is subjected to a car's rear end and the behaviour of the bumper will be analyzed. GISSMO's accuracy will be the primary measurement for this load case. See Figure 43 and 44 to see the geometries of the two cases.

The global objective for this thesis is to find which of the models that are most suitable to use in car crash simulations. This is done by evaluating the accuracy of the result and the extra amount of time required to run a simulation with different material models. This report aims to work as guidance when choosing a failure model for car crash simulations.

2 Theory

2.1 Stress measures

Bridgman [3], Rice and Trace [16] have showed that material failure is dependent of the stress state. Hence, the stress state is necessary to take into consideration when characterizing a material's properties. When performing crashworthiness calculations, it is useful to describe the stress state of different load cases using the invariants of the stress tensor. Crashworthiness computations are often performed on a sheet metal structure and a common assumption for this structure is that plane stress prevails. If plane stress prevails, the different stress states can be uniquely determined with just one parameter. The parameter is called the triaxiality, η, and it is defined as

$$\eta = \frac{I_1}{\sigma_{eq}} \tag{1}$$

where I_1 is the first stress invariant

$$I_1 = \frac{\sigma_1 + \sigma_2 + \sigma_3}{3} \tag{2}$$

and σ_{eq} is the von Mises stress and $\sigma_1, \sigma_2, \sigma_3$ are the principal stresses.

$$\sigma_{eq} = \sqrt{\sigma_1^2 + \sigma_2^2 + \sigma_3^2 - \sigma_1\sigma_2 - \sigma_1\sigma_3 - \sigma_2\sigma_3} \tag{3}$$

Von Mises yield criteria is frequently used when considering materials with isotropic properties. It is formulated as

$$F(\sigma) = \sigma_{eq} - \sigma_y(k) \tag{4}$$

where $\sigma_y(k)$ is the yield stress as function of a hardening parameter, k. Yielding occur when $F(\sigma) = 0$.

2.2 Material testing

To understand what applications a certain material is suitable for, it is necessary to characterize its properties. To characterize a material's failure properties, different stress states have to be analyzed. This thesis involves analyzing the behaviour during five different material tests. These are one uniaxial tension test, two different shear tests and two different notched tests. These different tests are chosen because they cover a wide spectrum of stress states. The geometries of the specimens that are used in this thesis are visualized in Appendix, see Figure 38-42.

2.2.1 Uniaxial tension test

The most fundamental material properties can be obtained from a uniaxial tension test. It is performed by locking one end of the specimen and applying a predefined load to the other. The elongation of the specimen is measured until failure. With

known initial dimensions of the specimen and the measured elongation, the relationship between stress and strain can easily be obtained. Figure 1 shows a schematic stress-strain relationship, obtained from a uniaxial tension test. The material behave linear elastic until the yield point σ_y and the relationship between stress and strain in the loading direction until this point is described by Hooke's law i.e $\sigma = E\varepsilon$. If the material is loaded further, the material enter the plastic region. Askeland [2] describes the dislocation processes that cause the observable plastic behaviour. When the material is loaded into the plastic region, the yield stress rises. This kind of treatment is called strain hardening.

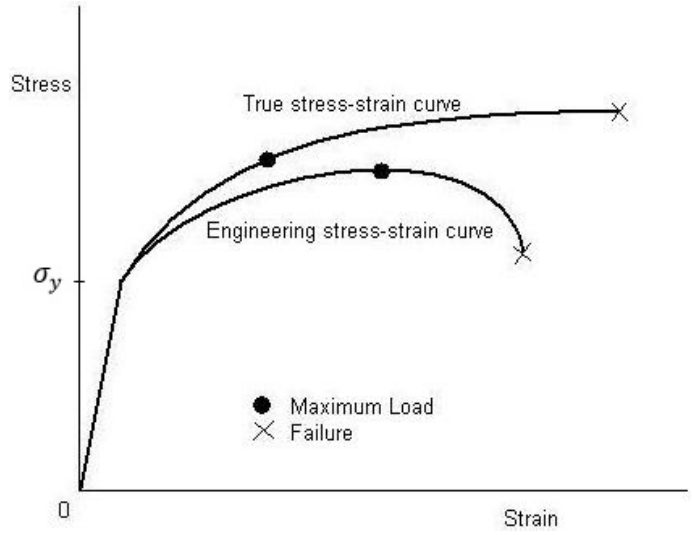

Figure 1: Typical stress vs. strain curve for a ductile metal.

Furthermore, at the ultimate tensile strength, the hardening of the material can no longer compensate for the decrease in area. See Figure 1, where the initiation of diffuse necking is marked as the maximum load. The softening that arises after this point, is due to the engineering measures. A problem with the engineering measures is that they do not consider that the dimensions change during loading. The uniaxial tension test specimen is assumed to deform uniformly before necking. Until this point, the engineering measures may directly be converted into true measures with the following relations

$$\varepsilon_{eng} = \int_{L_0}^{L_1} \frac{dL}{L_0} = \frac{\Delta L}{L_0}, \sigma_{eng} = \frac{F}{A_0} \tag{5}$$

$$\varepsilon_{true} = \int_{L_0}^{L_1} \frac{dL}{L} = ln(\frac{L_1}{L_0}) = ln(1 + \varepsilon_{eng}) \tag{6}$$

where F denotes force, A_0 is the initial area, L_0 is the initial length and, ΔL the difference in length per iteration. During uniform expansion the volume can be assumed to be constant and then the true stress can be calculated as:

$$\sigma_{true} = \frac{F}{A} = \frac{F \cdot L_1}{A \cdot L_1} = \frac{F \cdot L_1}{A_0 \cdot L_0} = \sigma_{eng} \cdot e^{\varepsilon_{true}} = \sigma_{eng}(1 + \varepsilon_{eng}) \tag{7}$$

where A and L are the current dimensions of the specimen.

The true strain consists of one elastic part and one plastic part. Equation 6 together with Hooke's law gives the true plastic strain as

$$\varepsilon_{true,plast} = \varepsilon_{true} - \frac{\sigma_{true}}{E} \tag{8}$$

which is valid until diffused necking occurs i.e at the maximum load. The physical interpretation of diffused necking is when the specimen no longer is deformed uniformly and the specimen suffer from a quick reduction of the width at a certain cross section.

2.2.2 Standardized material test

The geometry of the uniaxial test specimen can be either flat or circular, with standardized dimensions. Figure 2 and Table 1 define the geometry and dimensions of a flat specimen according to American Society for Testing and Materials [8].

Due to uncertainties regarding the exact properties of the material used in the

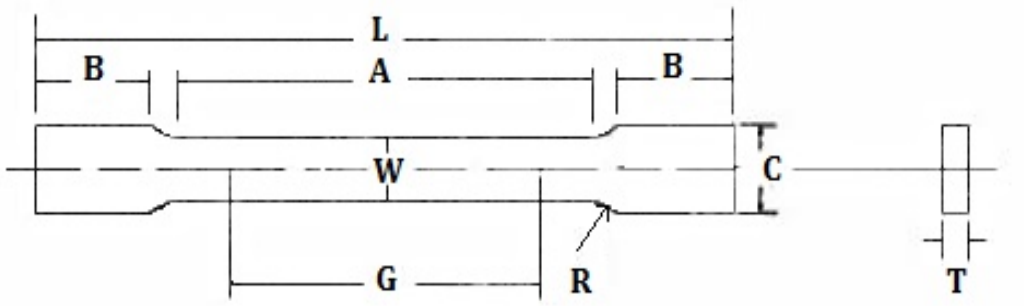

Figure 2: A specimen suited for uniaxial tension test with standardized dimensions. Figure reproduced from [8]

Table 1: Dimensions to Figure 2

A - Length of reduced section	57.15 mm.
B - Length of grip section	50.80 mm.
C - Width of grip section	19.05 mm.
G - Gage length	50.80 ± 0.13 mm.
W - Width	12.70 ± 0.25 mm.
T - Thickness	Thickness of the material
R - Radius of fillet	12.70 mm.
L - Over-all length	203.2 mm.

specimen, there could be deviations between the response of two geometrically identical specimens that is subjected to the same loading. Thereby, to make sure the

results are reliable, it is recommended to do a series of tests and compare the results. However, since CEVT has not got any experimental data available at this time, the material testing is completely done by computer simulations. The same specimens are used together with the different material models.

2.3 Strain rate dependency

Nowadays, there are a number of different materials in a car, each with its own properties. It is not uncommon that the response of the material is dependent of the loading rate, i.e the strain rate. A strain rate dependent material could have properties shown in Figure 3. However, the difference of Young's modulus, i.e the slope for the elastic behaviour, is very small for metals. Displaying that the higher strain rate the material is subjected to, the stronger it behaves. To understand if a material will show this property or not, it is necessary to know how the material has been treated previously. There are a few factors that decide if the material, in this case steel, is strain rate dependent. Firstly, it depends on which materials the steel is composed of. It also depends on the thermal treatment that the steel has been subjected to. The temperature of the material is also important to know.

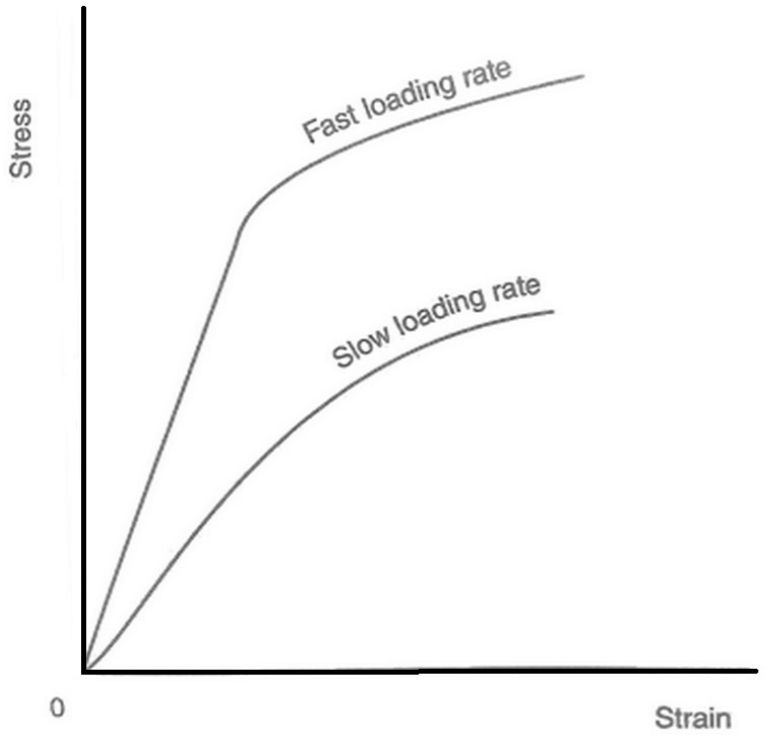

Figure 3: The true stress plotted as a function of true strain to show the influence of the strain rate.

2.4 Damage mechanics

Damage is a central part of the material properties when considering material failure. The concept assumes growth of voids in the material. The damage, D, is basically a measure for the reduction of the cross section area with respect to the upcoming voids, see Figure 4.

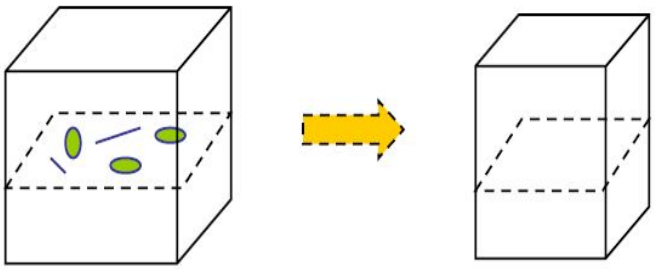

Figure 4: The current section area and the effective section area. Figure reproduced from [10].

Figure 4 shows the overall section area including micro defects and the reduced, effective, section area. If A represents the current section area, i.e the cross section area including the area of the voids, and A_{eff} represents the effective cross section area, i.e. the cross section area excluding the area of the voids, Lemaitre and Chaboche [12] define the damage parameter as follows

$$D = 1 - \frac{A_{eff}}{A} = \frac{A_{defect}}{A} \tag{9}$$

$$A_{defect} = A - A_{eff} \tag{10}$$

When the damage equals 1, the material fails. The reduction of the cross section has an effect on the stress used to model the global response. The definition of σ_{true}, see equation 7, together with equation 9 above gives Lemaitre's formulation [12] which is a basic relation to couple damage to the stresses

$$\sigma_{eff} = \frac{F}{A_{eff}} = \frac{\sigma_{true}}{1-D} \Rightarrow \sigma_{true} = (1-D)\sigma_{eff} \tag{11}$$

This is basic damage theory and the fundamentals for the different failure models. One common difference between the models is the damage evolution. Liang Xue [19] claims that one of the most commonly used and simplest ways of describing the damage evolution is the Johnson Cook model that yields

$$\dot{D} = \frac{\dot{\varepsilon}_p}{\varepsilon_f} \tag{12}$$

where the damage evolution is proportional to the equivalent plastic strain rate, $\dot{\varepsilon}_p$ and ε_f is the equivalent plastic strain at failure. Besides this, there are other damage evolution laws that are used e.g. the evolution law used in GISSMO.

2.5 Explicit analysis

To solve time dependent ordinary differential equations (ODE) and partial differential equations (PDE) with finite element analysis, either an explicit or an implicit method is used. For example the equation of motion that is given by

$$\mathbf{M}\ddot{\mathbf{a}}_n + \mathbf{f}_{int}(\mathbf{a}_n) = \mathbf{f}_n \tag{13}$$

where $\mathbf{M}$ is the mass matrix, $\mathbf{f}_{int}(\mathbf{a}_n)$ is the internal forces, $\mathbf{f}_n$ is the external forces, $\mathbf{a}_n$ is the displacement, $\ddot{\mathbf{a}}_n$ is the acceleration and index n represent the current time step where the nodal values is known. The explicit method implies that instead of solving for $\mathbf{a}_n$ it solves for $\ddot{\mathbf{a}}_n$. By doing this, the solving of the inverse of the stiffness matrix which is included in $\mathbf{f}_{int}(\mathbf{a}_n)$ is avoided. Yang et al. [20] claims that this is an advantage since solving the inverse could be demanding when considering big systems.

According to Ottosen and Ristinmaa [15], Newmark's time integration scheme may be used to solve equation 13 for $\ddot{\mathbf{a}}_n$ and the integration scheme reduces to the following:

$$\mathbf{a}_{n+1} = \mathbf{a}_n + \dot{\mathbf{a}}_n \Delta t + \frac{\Delta t^2}{2}\ddot{\mathbf{a}}_n \tag{14}$$

$$\dot{\mathbf{a}}_{n+1} = \dot{\mathbf{a}}_n + \frac{\Delta t}{2}(\ddot{\mathbf{a}}_n + \ddot{\mathbf{a}}_{n+1}) \tag{15}$$

where Δt is the time step and the nodal values with index n are known. With these two equations, it is possible to obtain an expression where $\ddot{\mathbf{a}}$ is expressed in terms of $\mathbf{a}$, see [15] for details.

$$\ddot{\mathbf{a}}_n = \frac{1}{\Delta t^2}(\mathbf{a}_{n+1} - 2\mathbf{a}_n + \mathbf{a}_{n-1}) \tag{16}$$

If equation 16 is inserted in equation 13 it is reformulated as

$$\mathbf{M}\mathbf{a}_{n+1} = \mathbf{M}(2\mathbf{a}_n - \mathbf{a}_{n-1}) + \Delta t^2(\mathbf{f}_n - \mathbf{f}_{int}(\mathbf{a}_n)) \tag{17}$$

Where the nodal values of index n and n-1 are known and the internal forces can be determined. Also since explicit method usually use lower order elements, $\mathbf{M}$ will be a diagonal matrix, meaning that the inverse of the mass matrix is trivial. Hence, a nonlinear dynamic problem as for example, elastic-plastic material behaviour can be solved directly without iterations. However, the simplification has its disadvantage, which is that the solving technique is only conditionally stable. If the solution becomes unstable the error will rapidly increase with every time step and the solution will become invalid. An explicit method usually needs to have 100 to 10000 times smaller time steps than an implicit technique, that is unconditionally stable, to avoid this kind of error. The time step for this method is limited by the time it takes for the shock wave, that arises from the loading, to transmit through the smallest element in the mesh

$$\Delta t = \frac{d_{min}}{c} \tag{18}$$

where d_{min} is the smallest distance between any two nodes in an element and c is the sound speed in the material. The speed of sound is computed as

$$c = \sqrt{\frac{E}{\rho(1-\nu^2)}} \tag{19}$$

where E is Young's modulus, ρ is the mass density and ν is Poisson's ratio. The solving method does not allow the shock wave to transmit a longer distance than d_{min} during Δt and regulates this by slowing down the sound speed by increasing the mass density of this element. Thereby, to prevent the solution for becoming unstable, the mass density of the element is raised. See LS-DYNA - theory manual, chapter 22 [9] for more details.

The implicit method on the other hand is iteratively converging to equilibrium in every times step and for complex problems this will be expensive. This means that when viewing car crashes, which is a complex dynamic load case during a short time period, an explicit method is preferable.

3 Material modelling

3.1 LS-DYNA

The capabilities of LS-DYNA are many and includes dynamic- and static computations, material failure analysis and crack propagation to name a few. LS-DYNA's explicit solving technique is widely used in the automotive industry. One reason for this is that it predicts the car's behaviour and effect upon the occupants during collision.

To run a simulation, a ".key"-file is needed. The key-file is a script that contains a series of keywords. The keywords inform the solver about how the simulation is supposed to be performed such as which geometry, material model, boundary conditions, time step, etc. that are wanted. The objective is to replace CrachFEM with GISSMO when simulating material failure behaviour. The keywords that will be used instead of these are *MAT_024, which model the elasto-plastic behaviour, and *MAT_ADD_EROSION, which model material failure.

3.1.1 *MAT_024

*MAT_024 is an elasto-plastic constitutive model based on von Mises yield criteria which is used to model the material behaviour until the point where instability occur. The input parameters implemented in the *MAT_024 card are primarily Young's modulus, the mass density, Poisson's ratio and the hardening of the material. The hardening curve shall only cover the loading path until instability initiates.

Furthermore, the model supports more complex material behaviour where the material is strain rate dependent, i.e a visco-plastic model. Instead of implementing one hardening curve, a table defining different strain rates which are connected to a certain hardening curve has to be implemented to capture the behaviour. However, *MAT_024's properties are not able to express the material behaviour beyond the point of uniform expansion. To be able to obtain that part of the behaviour, the *MAT_ADD_EROSION keyword is used.

3.1.2 *MAT_ADD_EROSION

Several of the constitutive models in LS-DYNA do not allow material failure. The *MAT_ADD_EROSION keyword provides an optional method to add these properties to other material models. The keyword includes options to implement GISSMO.

LS-DYNA User's Manual Volume II [13], gives a detailed description of the input parameters, but a few of the most important and critical parameters are presented in Table 2 below. These are the parameters that have to be identified through reversed engineering with a optimization software, LS-OPT.

Table 2: Table covering some of the most critical input parameters for GISSMO

LCSDG	Load curve defining the relationship between triaxiality and equivalent plastic strain at failure
ECRIT	Load curve defining the relationship between triaxiality and critical equivalent plastic strain.
DMGEXP	Exponent for nonlinear coupling of damage.
FADEXP	Exponent for damage related stress fadeout.
LCREGD	Load curve defining the relationship between the element size and scalars. To make the model independent of the mesh size.

To implement the model and make it valid not only to standardized material tests, but also to car crash simulations, the input parameters need to be determined using a variety of tests. The tests should be covering the whole spectrum of values of η, or at least cover the tension spectrum described in the Table 3.

Table 3: The interpretation of different stress states

Load case	**Triaxiality**
Pure shear	0
Uniaxial tension	1/3
Biaxial tension	2/3

3.2 LS-OPT

LS-OPT is used to calibrate the properties of the material modelled in LS-DYNA. The optimization program compares the force-displacement relationship modelled by GISSMO and *MAT_024 with the reference material. In this case, the reference behaviour is obtained from simulations with MF GenYld+CrachFEM. LS-OPT tries to minimize the difference between these with a chosen optimization method. One commonly used method is the Mean Square Error technique, MSE, which measures the differences of the two function values. The method that is used to do the optimizations in this thesis is called Partial Curve Matching, PCM. The PCM method evaluate the area between the curves, instead of just the vertical distance. This method is used since it works better than others when the curve has a steep slope, which most of the material tests have. Witowski, Feucht and Stander [18] describe the optimization method in further detail.

3.3 Material failure

When doing calculations on material failure, it is important to know how the material model evaluates material failure. Most of the models are tension based, that mean that failure do not occur during compression. There are two commonly used methods to do this. The first method is said to be a *failure criteria*. A failure criteria predicts a point of failure but does not model the actual failure behaviour. If the damage of

an element exceed a certain safety value, the element is eliminated. A failure criteria is also defined as a failure model which does not couple damage with the stress. The second method is called *failure model*, which instead of just eliminating the element, tries to realistically analyze the rupture path and lower the loading capacity of an element continuously in proportion to its damage parameter, i.e couple the damage to the true stress.

CrachFEM is a failure criteria, since when the failure has initiated, the propagation goes really fast and some people mean that the interesting part is to know if the material will fail. New trends contradict this, meaning that it is of importance to predict the propagation as well. GISSMO uses a failure model, and hence, supports this prediction. Thereby, GISSMO has a potential advantage against CrachFEM, but since this thesis implements GISSMO with data generated by CrachFEM and not from experimental results, the property is lost.

Figure 5 displays the difference between the two methods with a true stress - true strain relation. The green curve, display the relation of a failure criterion, where the damage is not coupled to the stress. The red curve displays the stress - strain relation of a failure model, where the damage is coupled to the stress.

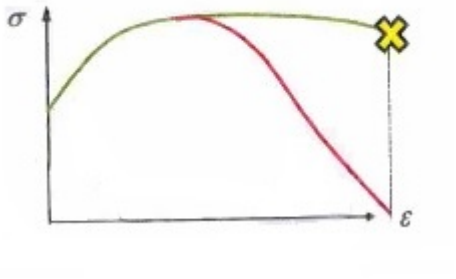

Figure 5: The difference between when the damage is coupled or uncoupled from the true stress. The figure is reproduced from DYNAmore.

3.3.1 MF GenYld+CrachFEM

MF GenYld+CrachFEM defines a material model, built of MF GenYld which model the elasto-plastic behaviour and CrachFEM which model material failure. This is a failure criteria and should be used to predict *when* failure occur, and not to predict the rupture path. The following is a short version of the theory behind MF GenYld+CrachFEM, for further details, see MF GenYld + CrachFEM 4.2 User's Manual [5].

This thesis only examine steels, meaning it is assumed that MF GenYld uses von Mises yield criteria and isotropic hardening seen in equation 4. However, MF GenYld

supports other yield criterion such as Hill that alter Von Mises to an anisotropic criteria and which is sometimes used for rolled steel. This is to meet the material behaviour of high-strength steel which can behave differently in biaxial tension compared to biaxial compression etc. Figure 6 displays an example of a modified yield surface that could be used to compensate for the anisotropic behaviour. MF GenYld model this material behaviour with so called yield locus correction seen in Figure 6. The correction is to adjust the yield criteria by:

$$k(\eta)F(\sigma) = \sigma_{eq} \tag{20}$$

where k is a stress-state dependent correction factor to reshape the von Mises yield criteria.

CrachFEM is a failure criteria divided in two different fracture criterion and if a

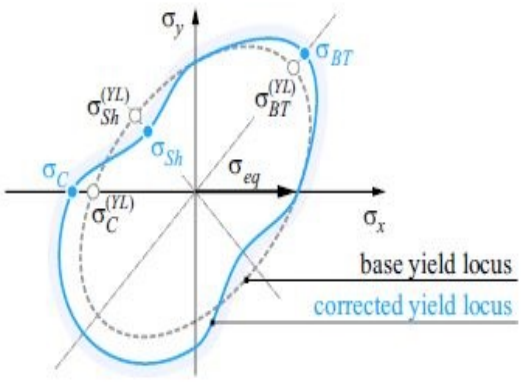

Figure 6: Examples of a yield surface in MF GenYld. Figure reproduced from CrachFEM User's manual. [5]

shell structure is considered a third fracture criteria is added to remediate lost information in the thickness. The criterion evolve separately and are assumed not to affect each other. Figure 7 presents the different criterion and how they are acting. The fracture criterion only occurs in tension and not in compression.

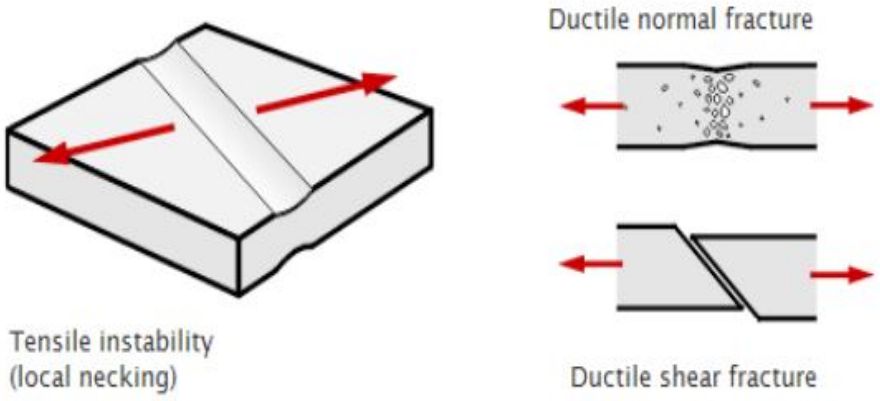

Figure 7: The difference between ductile normal fracture, ductile shear fracture and local necking. Figure reproduced from matfem.de

CrachFEM defines the three fracture modes with a fracture risk, ψ, which is dependent on the equivalent plastic strain ε_M and the plastic strain at fracture ε_M^*:

$$\psi = \frac{\varepsilon_M}{\varepsilon_M^*} \tag{21}$$

ε_M^* is here the fracture strain at a constant stress state. However, since the stress state usually changes during loading, the fracture risk has to change more consistently with changes of stress state:

$$d\psi = \sum_n^N \frac{\varepsilon_M}{\varepsilon_M^*(\sigma_{ij}^n)} \tag{22}$$

where N denotes the total number of time steps and σ_{ij}^n denotes the stress state in the current time step. When the fracture risk equals the fracture criteria $\psi^* \equiv 1$, then failure will occur.

The difference between the three fracture criterion is basically their way to determine ε_M^*. The ductile normal fracture criteria, seen in the upper right corner of Figure 7, examines the growth of micro voids that damage the material. During plane stress conditions, the ductile normal fracture determines the equivalent plastic strain at failure as a function depending on the triaxiality and the plastic strain rate, $\varepsilon_M^*(\eta, \dot{\varepsilon}^p)$.

The second fracture criteria called shear fracture is seen in the bottom right corner of Figure 7. Shear fracture occurs due to growth of shear band localisations. Shear fracture has a smooth fracture surface and fracture occur at a 45 degrees angle to the load direction compared to normal fracture that has a rough fracture surface and fracture perpendicular to the load direction. Ductile shear fracture determines the equivalent plastic strain at failure as a function depending on a shear stress parameter θ and the plastic strain rate, $\varepsilon_M^*(\theta, \dot{\varepsilon}^p)$.

$$\theta = \frac{\sigma_M}{\tau_{max}} \cdot (1 - k_{SF} * \eta) \tag{23}$$

$$\tau_{max} = \frac{\sigma_1 - \sigma_3}{2} \tag{24}$$

where k_{SF} describe how triaxialitiy effect shear fracture and τ_{max} is the maximum shear stress.

The last criteria is the ductile instability fracture seen to the left in Figure 7. The ductile instability fracture evaluates the instability through the thickness. The equivalent plastic strain at onset of fracture risk is a function of the in-plane deviatoric stress ratio, α and the strain rate, $\varepsilon_M^* = \varepsilon_M^*(\alpha, \dot{\varepsilon}^p)$.

$$\alpha = \frac{\sigma_2}{\sigma_1} \tag{25}$$

3.3.2 GISSMO

Focus has been directed to improve the prediction of crack initiation and propagation. To achieve this, Daimler and DYNAmore have tried to find a way where it is possible to determine and accumulate the pre-damage caused during the sheet metal forming to the crash analysis. The problematic part has been that an anisotropic yield criteria e.g. Hill [11] or Barlat [6] is used during the forming process and an isotropic yield criteria e.g. von Mises is used during crash simulations. A damage model that is suitable for both disciplines therefore has to correctly predict damage regardless of the yield criterion used. GISSMO has been developed to fill this gap by enabling mapping of damage and other various history parameters from the forming simulation to the crash simulation, see Figure 8.

GISSMO predicts failure by evaluating the damage parameter in equation 9. The

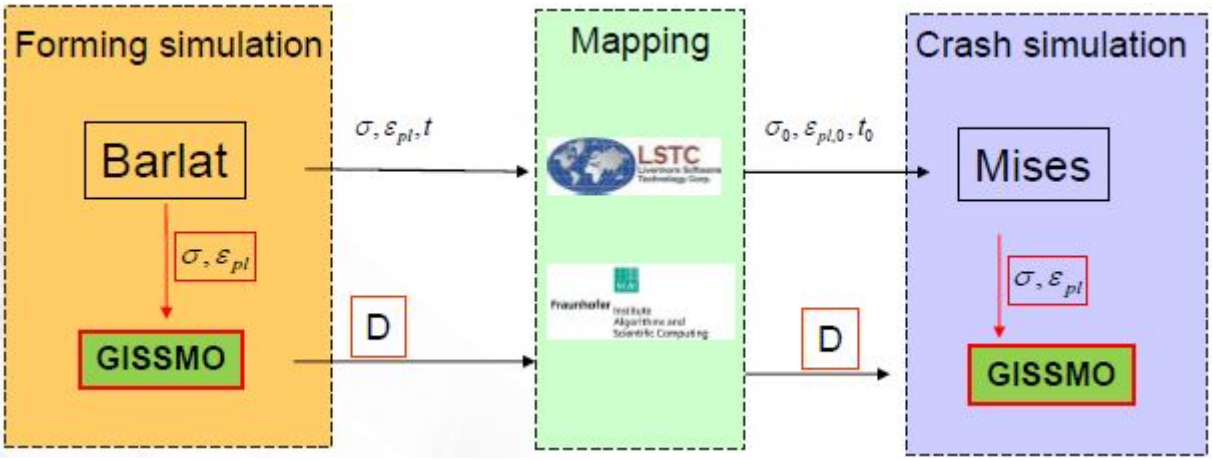

Figure 8: A schematic description of how the damage is accumulated through the process stages by GISSMO.

damage evolution of GISSMO has similarities with the previously mentioned Johnson Cook damage model. The difference is that Johnson and Cook's model is describing

the evolution of the damage as a linear expression, but GISSMO describes it as an exponential function

$$\dot{D} = \frac{n}{\varepsilon_f} D^{1-\frac{1}{n}} \dot{\varepsilon_p} \tag{26}$$

where D is the current value of the damage, $\dot{\varepsilon_p}$ is the equivalent plastic strain rate, n is the damage exponent and ϵ_f is equivalent plastic stain at failure. If n=1, equation 26 is reduced to the Johnson Cook model, see equation 12.

One useful property of GISSMO is to accumulate a measure of instability, F. F evolves according to the following function.

$$\dot{F} = \frac{n}{\varepsilon_{crit}} F^{1-\frac{1}{n}} \dot{\varepsilon_p} \tag{27}$$

where ε_{crit} is the equivalent plastic strain when instability occur. When F=1, instability is reached and it is now assumed that the damage is coupled to the true stresses through

$$\sigma_{true} = \sigma_{eff}[1 - \left(\frac{D - D_{crit}}{1 - D_{crit}}\right)^m] \tag{28}$$

where D_{crit} takes the value of the damage parameter when F reaches 1. m is the fade exponent, which is calibrated to match experiments. If m=1 and D_{crit}=0 equation 11 is proved to be a generalized expression of equation 26. For further motivation, see reference [7] and [14].

4 Results

4.1 CrachFEM results

The results presented below are from material test simulations, where CrachFEM has been used as failure criteria. The results are presented for a boron steel, since the crash simulations that CEVT run often involves failure in this material. Although, it is important to clarify that the working process is suitable for all kind of steels.

4.1.1 Test specimen validation

First of all, it is important to see that the material tests cover a broad spectrum of the triaxiality range. This thesis is focused on failure during tension. Thereby, the tests should have a triaxiality between 0 and $\frac{2}{3}$. Figure 9 shows the relationship between triaxiality and equivalent plastic strain, where the variables are measured in the element where the failure initiates.

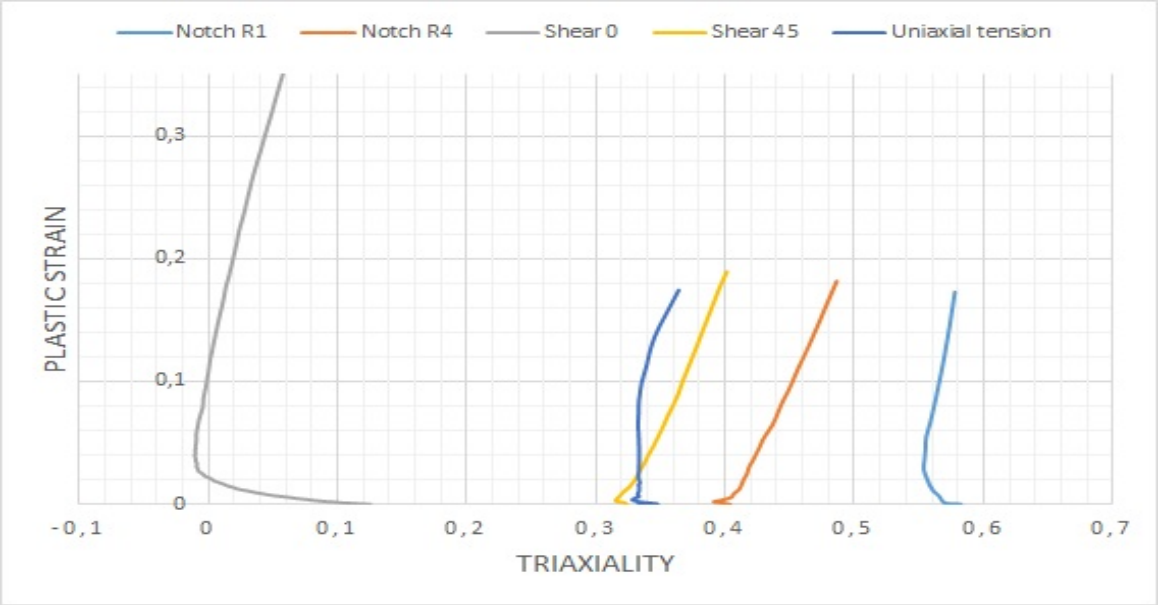

Figure 9: The relationship between the triaxiality and the equivalent plastic strain for the different test specimens.

It is difficult to achieve the theoretically correct stress states where for example a pure shear test should have triaxiality equal to 0 and a biaxial test equal to $\frac{2}{3}$. In Figure 9, the shear 0° test has a triaxiality around 0.06 at equivalent plastic strain at failure and the notch test with a radius of 1mm has a triaxiality around 0.57, which is considered to be ok. It would be good to minimize the triaxiality gap between the shear 0° and the uniaxial tension test, to be able to model the behaviour more accurately for stress states within these triaxialities.

4.1.2 Results from uniaxial tension test

Figure 10 shows a specimen during a uniaxial tension test at three different points in time. Boron steel has high strength and shows a stiff material behaviour compared to many other commonly used steels and as Figure 10 shows, there is almost no diffused necking before failure. The different color represent the equivalent plastic strains in each element. The specimen in the middle shows that the specimen is no longer deforming uniformly, which is an indication of diffused necking initiation.

Figure 11 shows the force-displacement curve generated with MF GenYld and CrachFEM. This curve is used as reference in the parameter identification process of GISSMO. The figure shows that the material does not allow any softening. This can be seen since the force is increased until the failure occurs. The steep slope in the end of the curve is not completely vertical though, but this can be explained by that the different elements in the cross section that have failed in Figure 10 do not fail at the exact same displacement.

Furthermore, boron steel is normally not strain rate dependent, which implies that the material has the same hardening behaviour for different loading rates. Figure 12 validates this assumption by displaying the hardening curve at two different loading rates, one of 0.1m/s and the other one at 10m/s. It may be noticed that the curve generated with the higher loading rate proceed further than the lower. This will not affect the following work, since the hardening curve is only valid until the maximum load. See Figure 1 for a reminder. However, the failure criterion of both CrachFEM and GISSMO are dependent of the strain rate, see section 2.6.2 and 2.6.3.

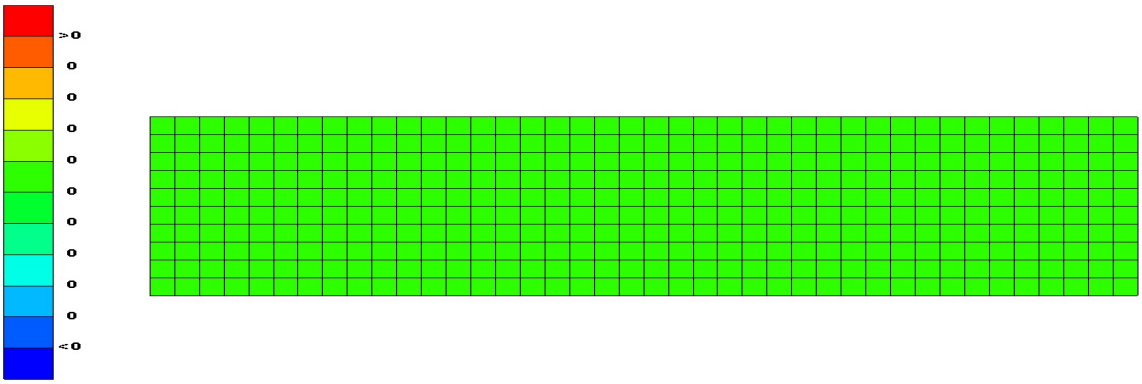

Undeformed specimen.

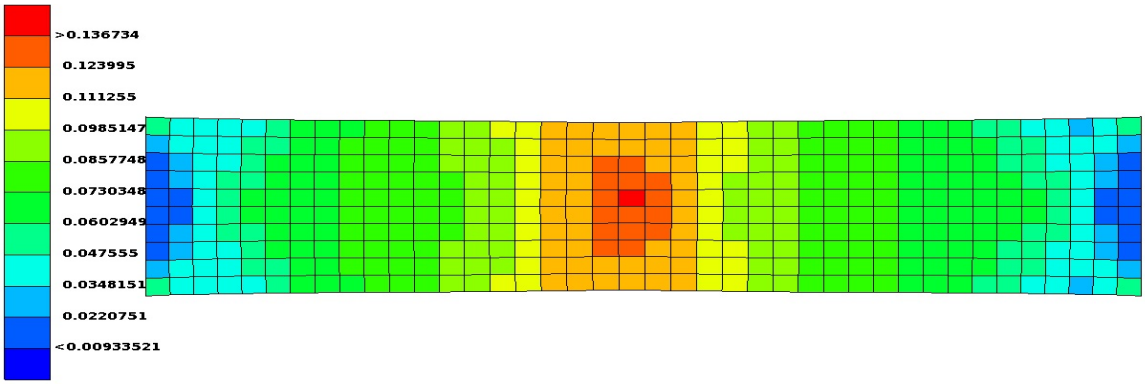

Diffused necking occur.

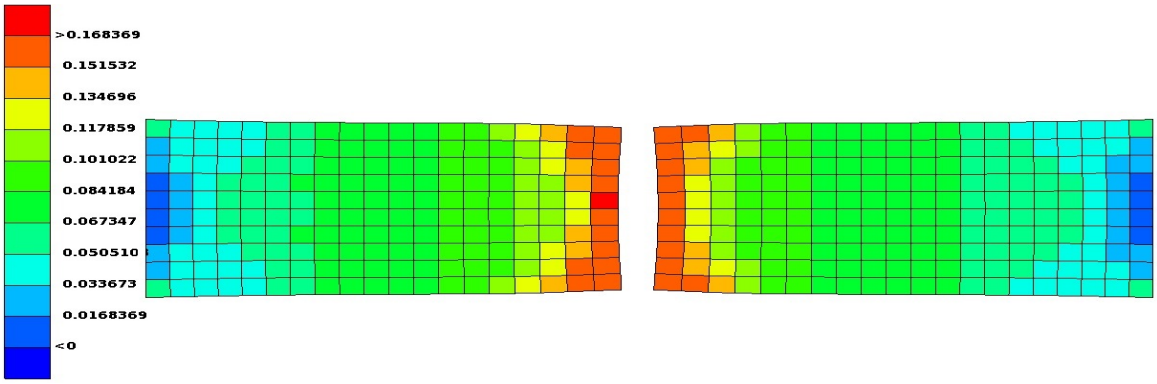

Failure occur.

Figure 10: Uniaxial tension test specimen at three different time steps during loading. The scale goes from blue to red, where red denotes highest values.

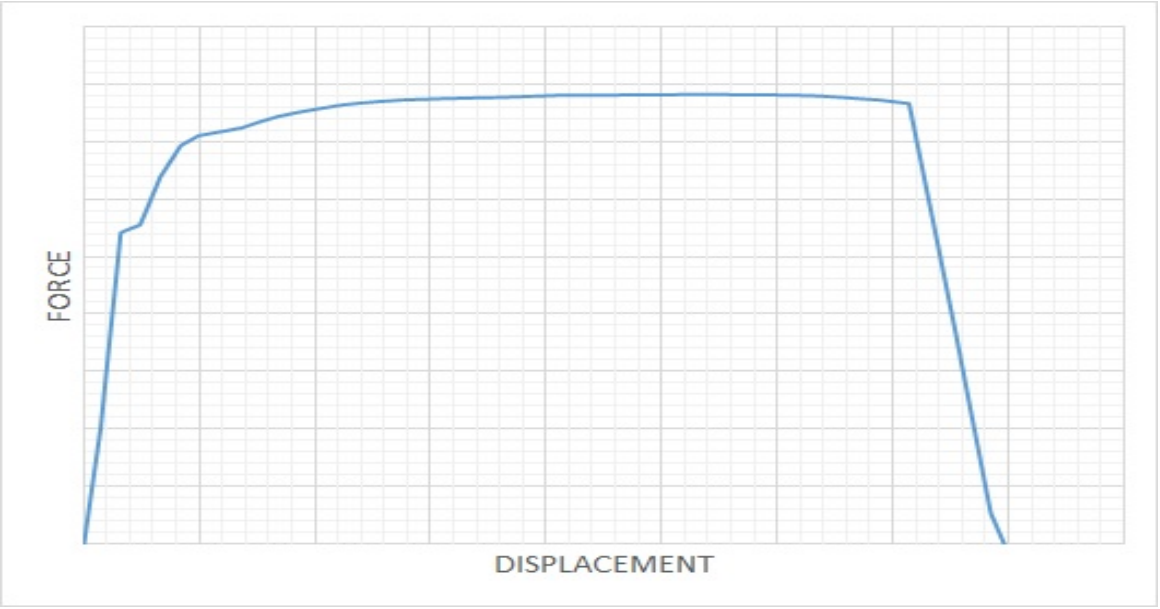

Figure 11: Force-displacement curve for a uniaxial tension test.

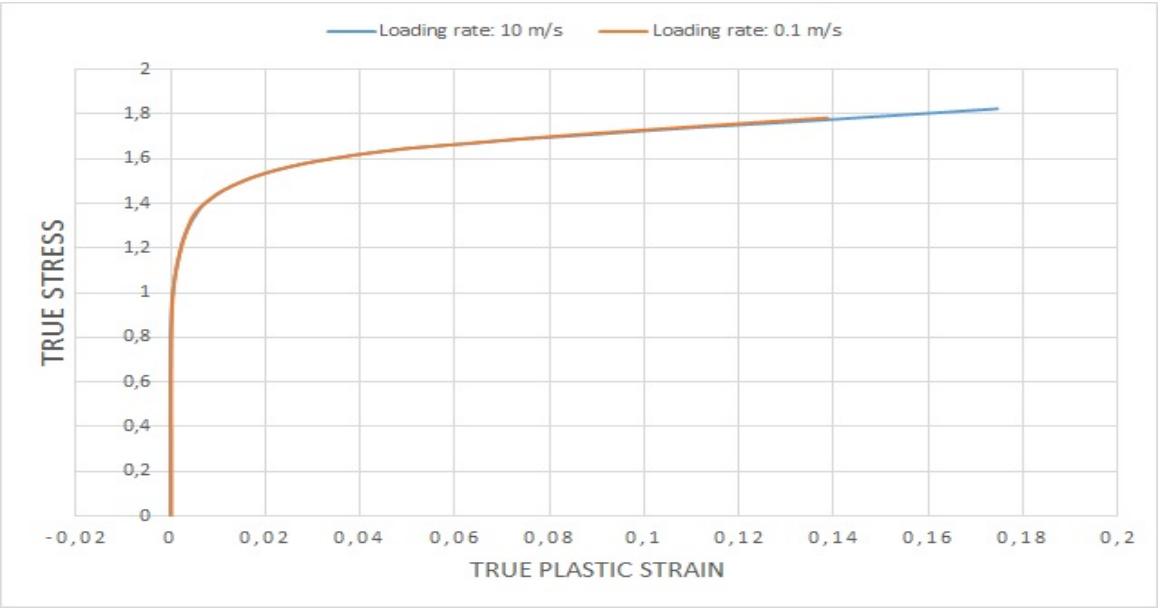

Figure 12: The hardening is identical at the different loading rates

4.1.3 Results from notch and shear tests

Computer simulations of the shear and notched tests have also been executed. Figure 13 displays the force-displacement relationships for these tests. This relation is used in the parameter identification process. It is only the part beyond the point where instability is initiated in these curves that is needed to calibrate GISSMO with LS-OPT since *MAT_024 models the elasto-plastic behaviour until that point.

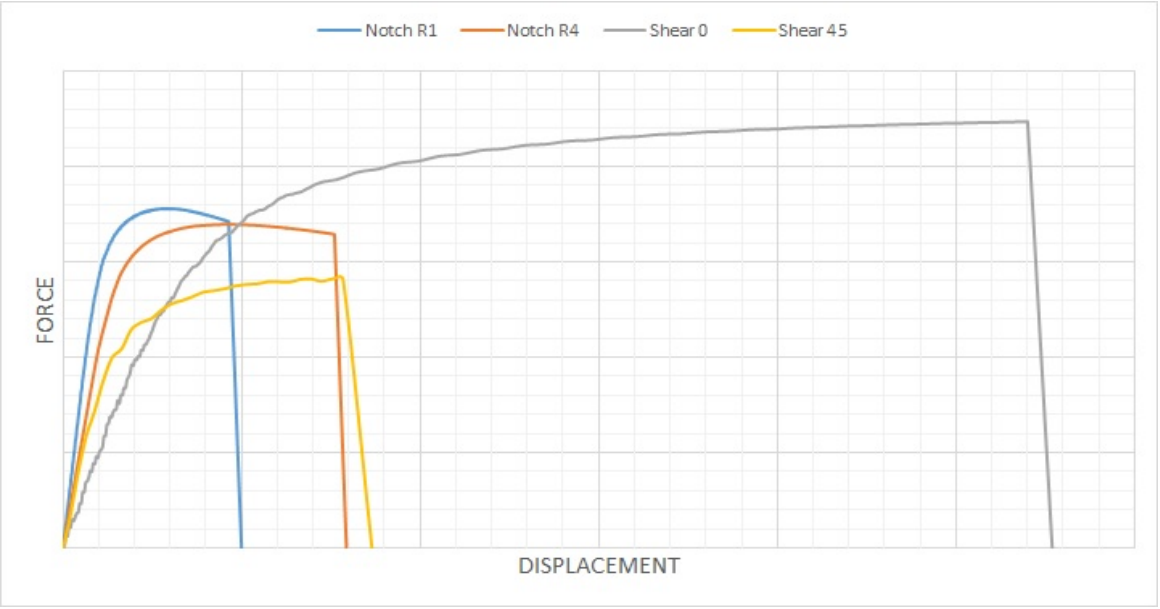

Figure 13: Force-displacement curves for Notch R1, Notch R4, Shear 0° and Shear 45°.

4.2 *MAT_024 results

The input parameters to *MAT_024 are the material's hardening curve, among other material constants. Figure 12 shows that this boron steel is independent of the strain rate, which simplifies the input of *MAT_024. This independence implies that one single curve will be valid for the material's hardening behaviour at any loading rate. The hardening curve in Figure 12 is used until the point where the assumption of uniform deformation no longer is valid. This point is determined by finding the maximum point for the engineering stress-strain relation, and then convert it to true values with equations in section 2.2.1.

4.2.1 Results from uniaxial tension test

A simulation with just the elasto-plastic material model is executed to verify that it has been implemented accurately. Since *MAT_024 does not include damage evolution, the ideal result would be that the response curves are matched until the diffused necking starts. At this point, the result from Crachfem should soften, or fail, with a higher rate than *MAT_024.

Figure 14 displays the force-displacement curve for a uniaxial tension test and prove the assumed behaviour. Figure 15 shows how the specimen is deformed during the loading at three different points in time. The different color represent the equivalent plastic strains in each element. Observe that the scale is not fixed, but changes during the loading. Since *MAT_024 does not include any material failure, the specimen starts to elongate with a high rate after diffused necking has occurred.

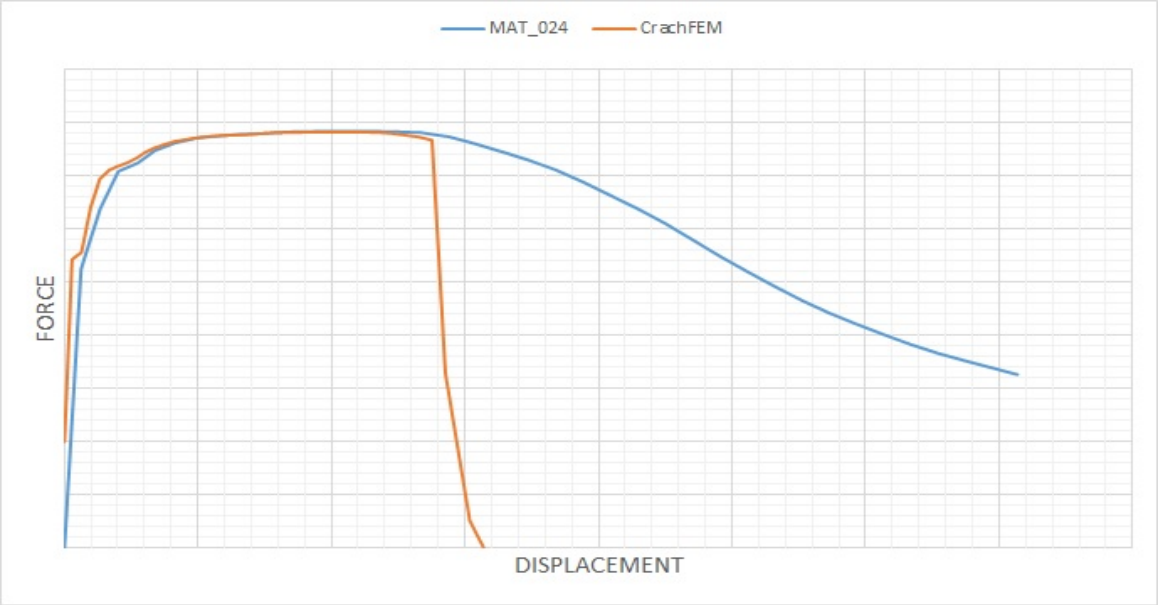

Figure 14: Force-displacement curves generated with a uniaxial tension test with Crachfem and MAT 24 respectively.

4.3 LS-OPT results

Five of the parameters in GISSMO have to be identified by reversed engineering through an optimization process. The parameters are the damage exponent, n from equation 26 and the fade exponent, m from equation 28. Furthermore, there are three different curves that also have to be defined, which are called ECRIT, LCSDG and LCREGD. The five of them are defined in Table 2. A more practical interpretation of ECRIT is that it states for which equivalent plastic strain the diffused necking should be initiated for different triaxialities, see equation 27. LCSDG defines for which strain failure shall occur for different triaxialities, see equation 26.

The first stage of the identification process is to run simulations for the five different specimens independently, picking out values for n and m and find approximate values for ε_{crit} and ε_f for the different test specimens, which have different triaxialities. The second stage is to run one optimization with all the different specimens together, to actually be able to establish the curves for ECRIT and LCSDG. The last stage is to make the material model independent of the mesh size, i.e to find the curve for LCREGD.

4.3.1 Result from uniaxial tension test

The first optimization is done for the uniaxial tension test. The relationship between force and displacement in Figure 11 works as a reference of how the same relationship

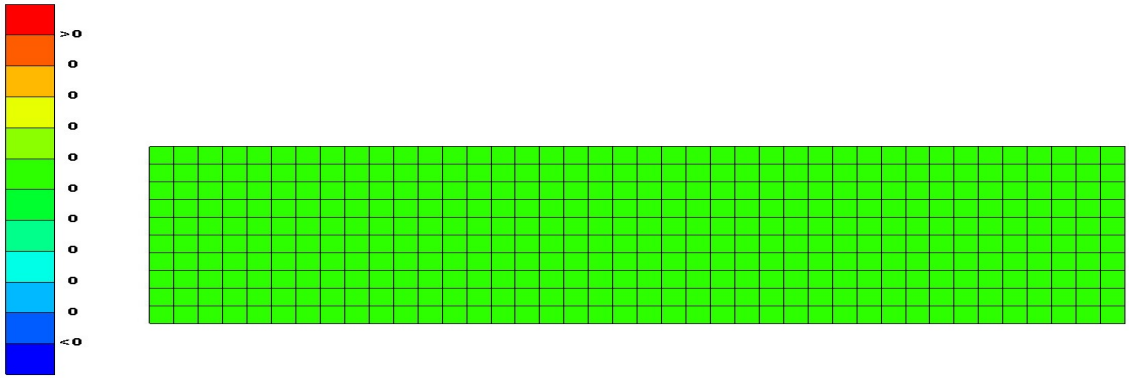

Undeformed specimen.

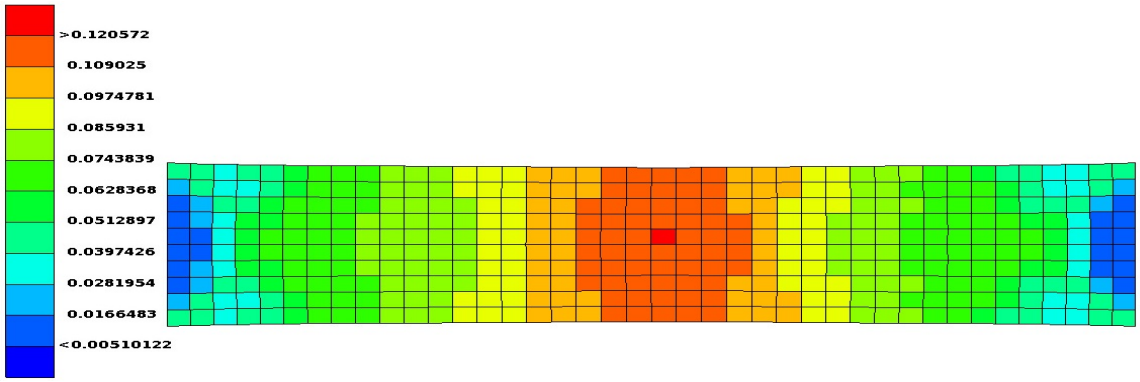

Diffused necking occur.

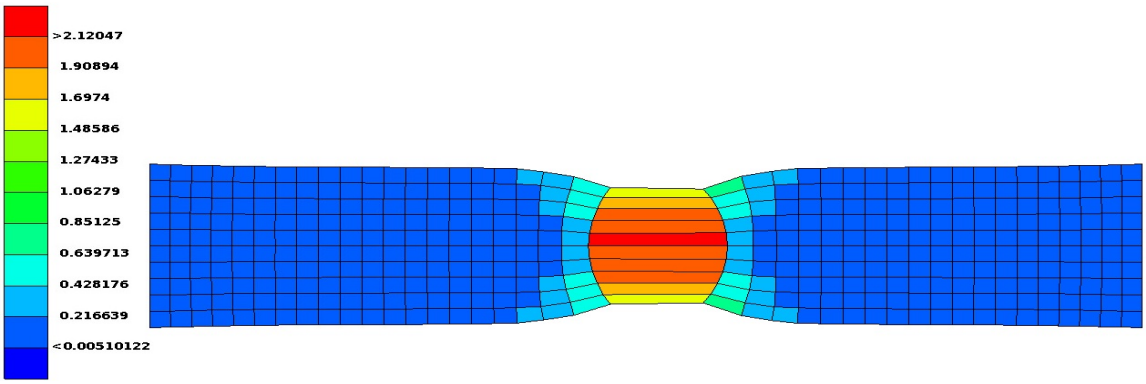

Failure does not occur.

Figure 15: Uniaxial tension test specimen at three different time steps during loading.

with GISSMO should look like. The values of the damage exponent, n and the fade exponent, m that are obtained from this optimization are not depending on the stress state. Thereby, these values will be used and will not be investigated any further. The values of ε_{crit} and ε_f will be used to build the ECRIT and LCSDG curve in the second stage. Figure 16 shows the result for the the uniaxial tension test. The "GISSMO v1"

is the curve obtained by the first simulation. The ”GISSMO FINAL” curve can be ignored for now.

The result with GISSMO correlate well with the result from CrachFEM.

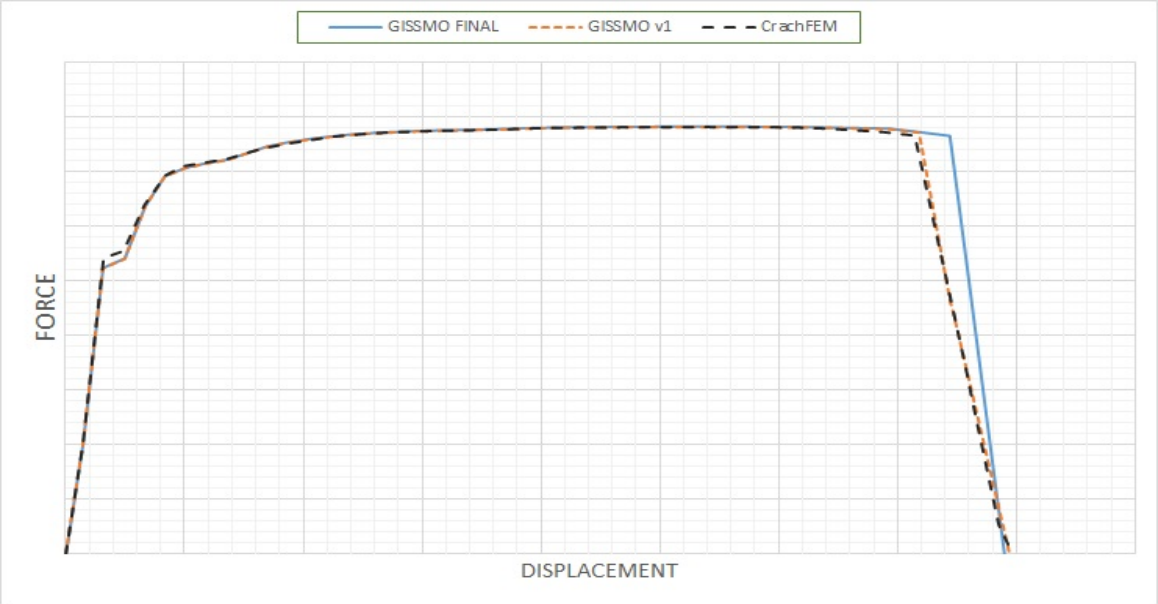

Figure 16: Force-displacement curve for a uniaxial tension test. Determined with GISSMO as a failure model.

4.3.2 Results from notch and shear tests

The four other specimens are then optimized, with the force-displacement curve relation as reference. ε_{crit} and ε_f are the only parameters during these optimizations. The results from these are presented in Figure 17 to 20 The ”GISSMO v1” curves show the results from these optimizations.

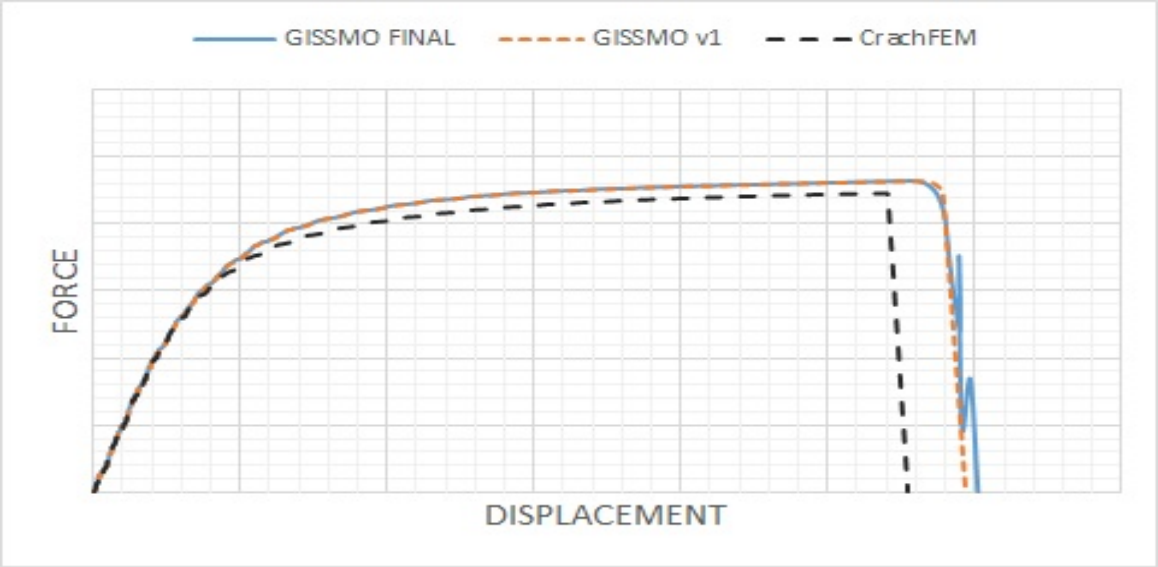

Figure 17: Force-displacement curve for a shear 0° test.

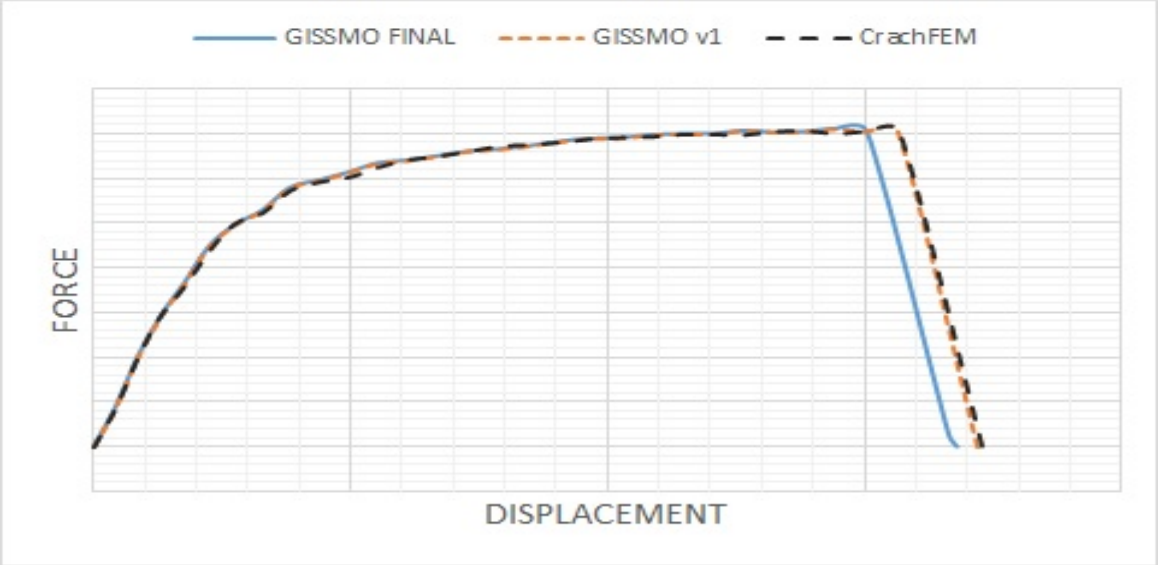

Figure 18: Force-displacement curve for a shear 45° test.

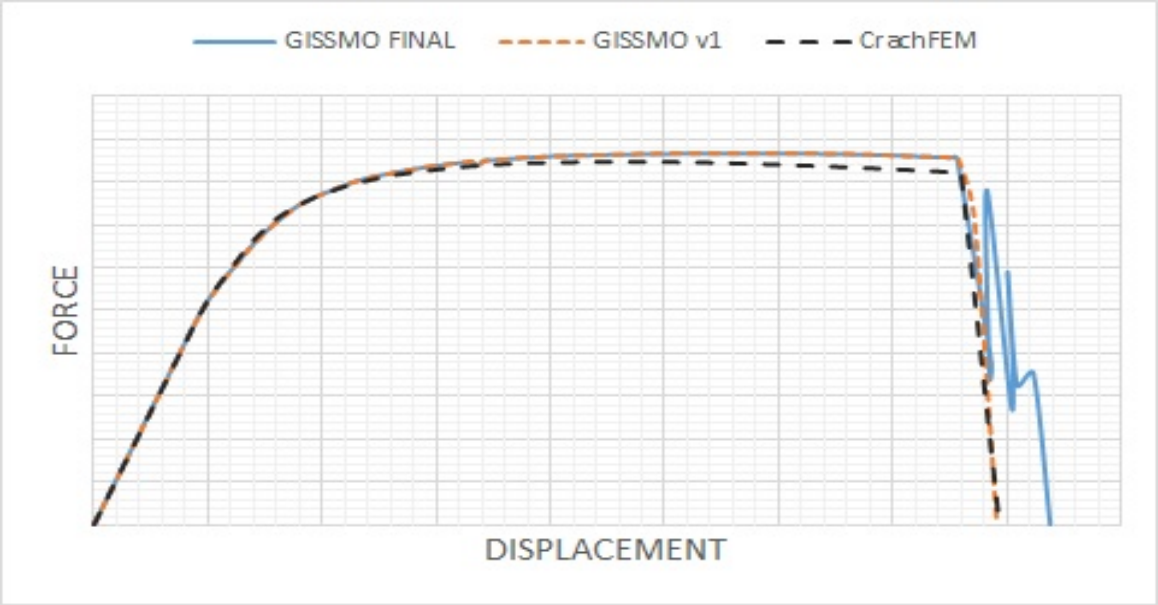

Figure 19: Force-displacement curve for a notch test with a notch radius of 4 mm.

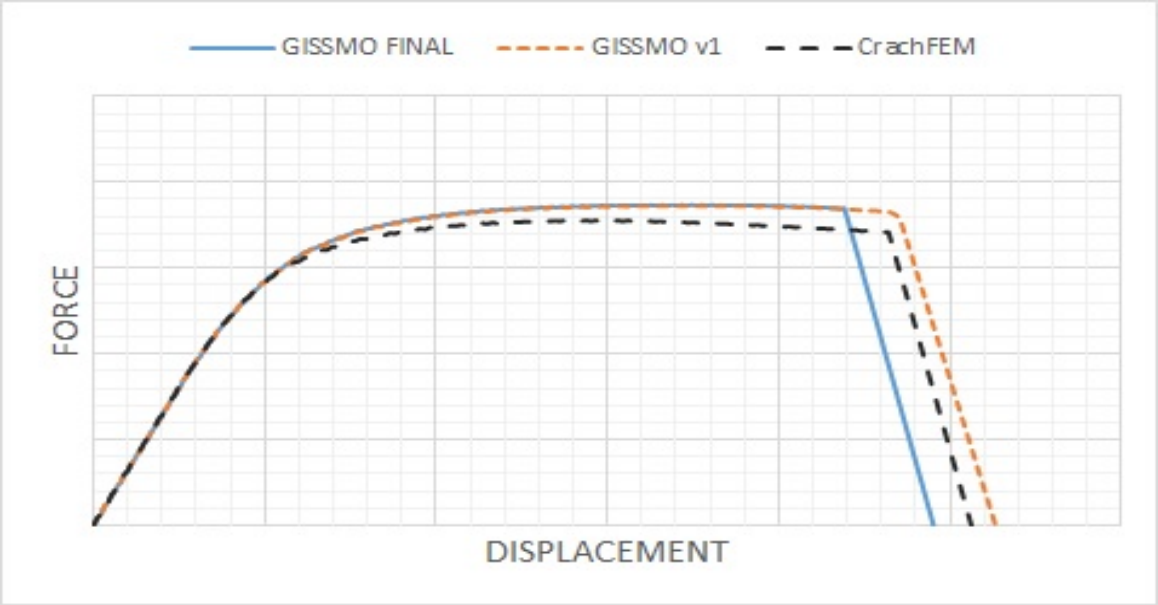

Figure 20: Force-displacement curve for a notch test with a notch radius of 1 mm.

4.3.3 Instability and failure calibration

The values of ε_{crit} and ε_f obtained in the first stage of the parameter identification give a hint of the range of the values for the final values of the points in ECRIT and LCSDG. The curves are built of six points with fixed triaxiality. The next step is to optimize the function values for the different triaxialities. In general, the result

is changed to the worse during this stage, which is what can be expected since the points that form the final ECRIT and LCSDG curves will be influenced by more than one test at the same time. The resulting curves for ECRIT and LCSDG are shown in Figure 21. It might seem strange that the ECRIT curve takes higher values than LCSDG at triaxialities between ≈0.35 to ≈0.62. This could be explained since the instability criterion in equation 27 is not fulfilled before failure i.e. $D = 1$. There are tendencies of this, since the specimen fail without any obvious necking behaviour. "GISSMO FINAL" in Figure 17-20 show the force - displacement relation with the final ECRIT and LCSDG curves. The results are generally worse than "GISSMO v1", and the results of the notch R4 and the shear 0° test in Figure 19 shows an unwanted failure behaviour due to the disruption in this stage. This disturbance may be due to the change of stress state of the remaining elements in the critical section when one of the elements fails. This behaviour disappears if the waist would contain more elements through its cross section or if the loading rate is reduced.

Figure 21: The relationship between critical plastic strain and triaxiality and the relationship between plastic strain at failure and triaxiality.

4.3.4 Regularization of element size

The last curve that has to be identified is the LCREGD curve. Figure 22 shows how the uniaxial tension test modelled with GISSMO is dependent of the element size. The results show that increased element size requires a higher elongation for failure. The identification of LCREGD initiates with the force-displacement curve and since no experimental data is available. Effelsberg et al. [7] propose an element size of 0.5 mm as reference, trying to make the other curves correlate with this as good as possible. Figure 23 shows the result and Figure 24 shows the LCREGD curve. The result shown in Figure 23 is approved for mesh sizes up to 5 mm. For some reason,

the element size of 10 mm is not regularized in the same extent that the other mesh sizes are. But since the others show good results and the most commonly used mesh size at CEVT is ≈3.5 mm, this should not be a problem.

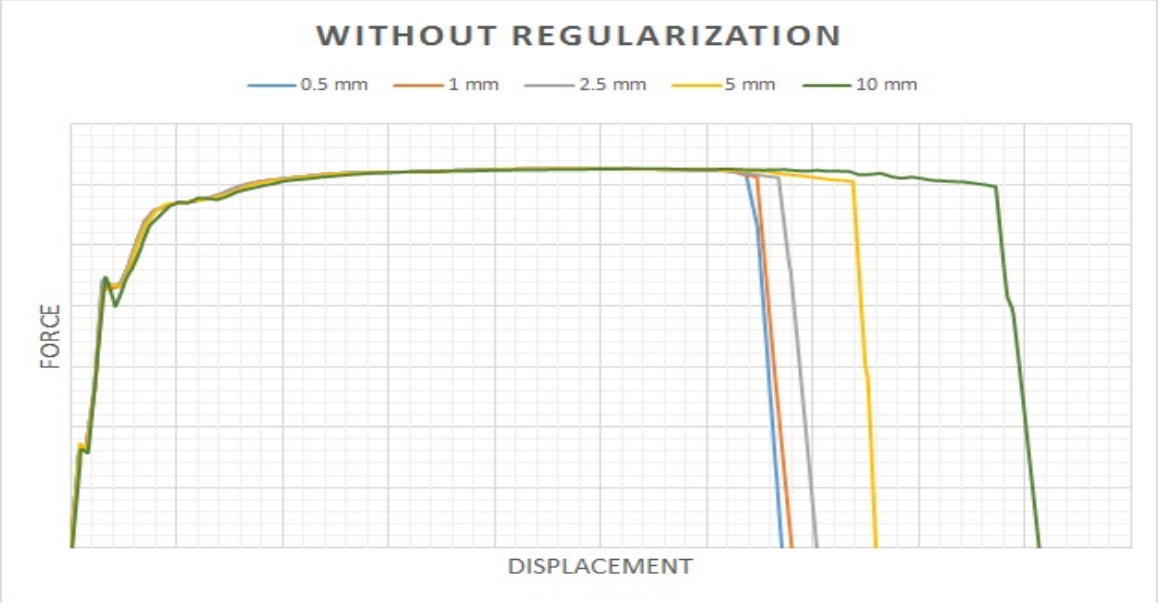

Figure 22: The relationship between force and displacement for a uniaxial tension test, simulated with five different mesh sizes.

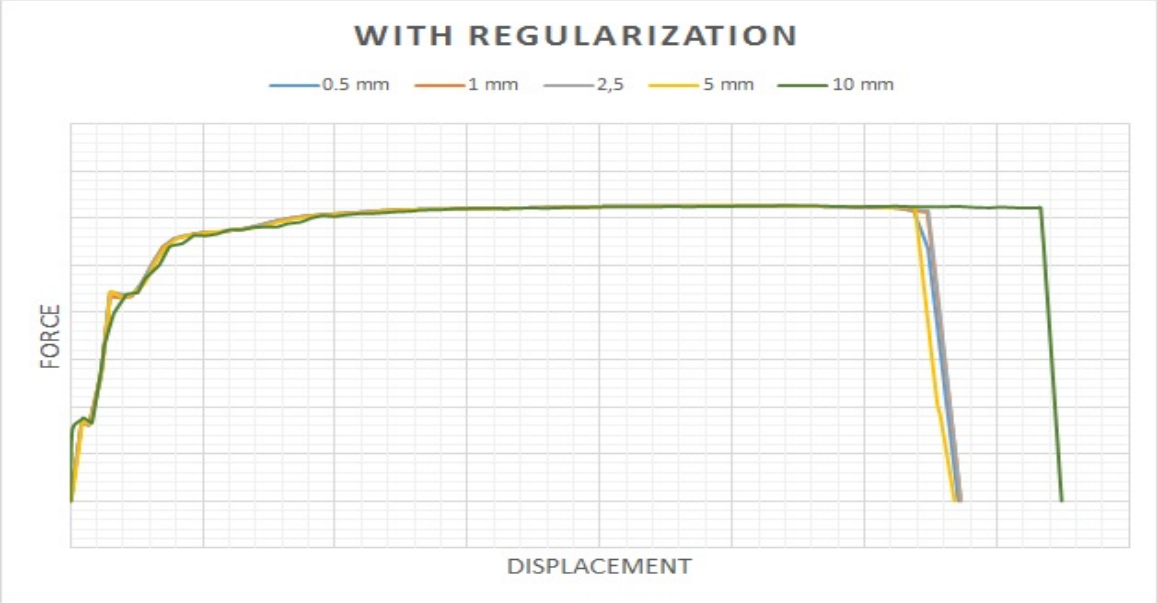

Figure 23: The regularized relationship between force and displacement for a uniaxial tension test, simulated with five different mesh sizes.

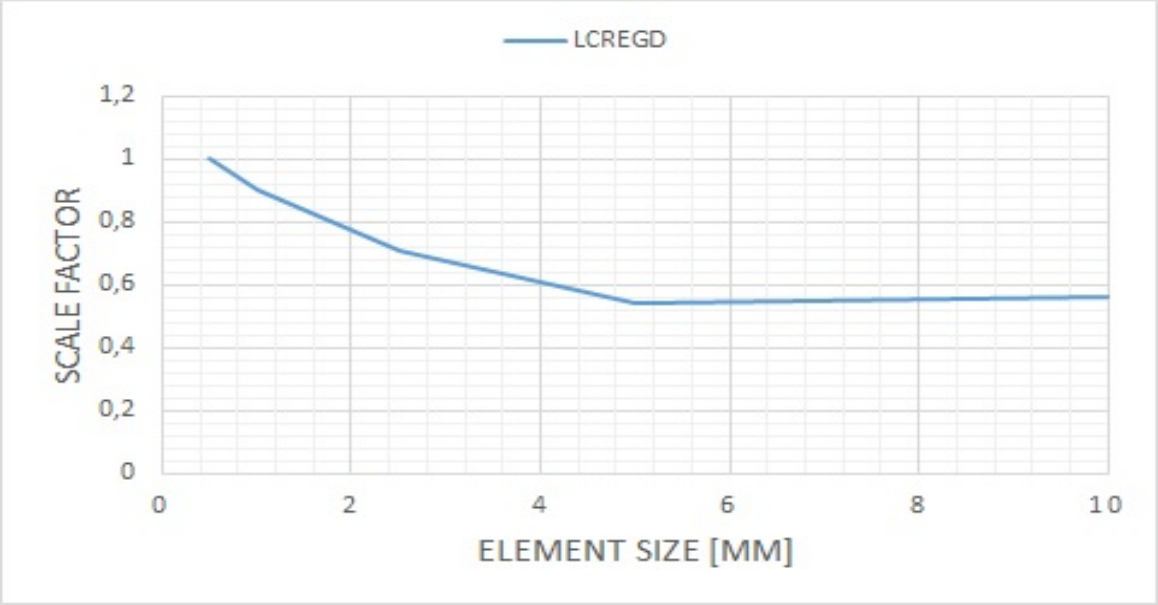

Figure 24: The relationship between a scalar factor multiplied to LCSDG and the element size, i.e the LCREGD curve.

4.4 GISSMO results

The critical factors of the material model are simulation time and material behavior. These factors will be investigated through two different load cases. The first test is of a B-Pillar and will focus on determining the potential reduction of the simulation time. The GISSMO and CrachFEM simulation will run on the same type of computer and with equally many CPU's to make the prerequisites identical. The second load case is of a rear car crash, where the behaviour of the rear bumper will be analyzed to investigate the accuracy of GISSMO.

4.4.1 B-Pillar

The B-pillar is built of a welded sheet structure which is simply supported by two cylinders. A third cylinder is placed above the pillar and between the two supports. The cylinders are regarded as rigid bodies and the upper cylinder is subjected to a vertical displacement downwards, deforming the beam until it fails. See Figure 43 in the Appendix for a visualization of the geometry. The material around the weld is weakened due to the welding and the area is called a "Heat Affected Zone", HAZ. This material has also been implemented within GISSMO through its own parameter identification process.

Figure 25 and Figure 26 show how the pillar is deformed and the failure behaviour modelled with CrachFEM and GISSMO respectively. The colors of the elements are dependent of the plastic strain value. There are some differences between CrachFEM and GISSMO after full loading which could be explained by that the damage parameter, for the elements in the critical zone, measured with CrachFEM arises quickly

after the first element fails, but the parameter is not coupled to material failure at the same way as GISSMO.

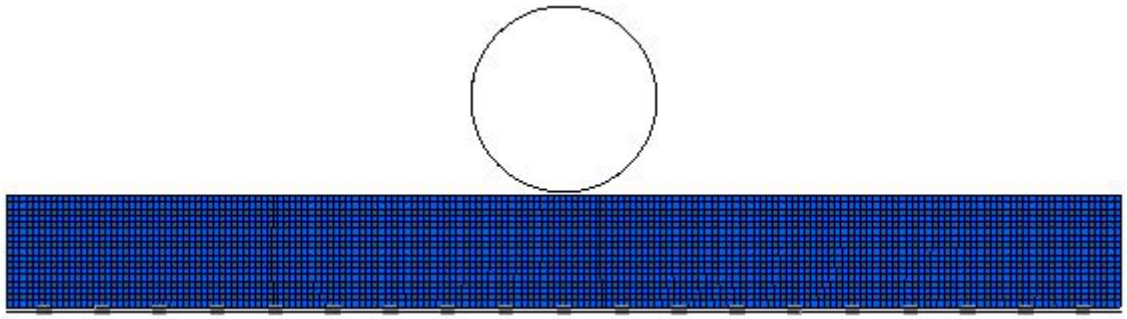

Before loading is applied.

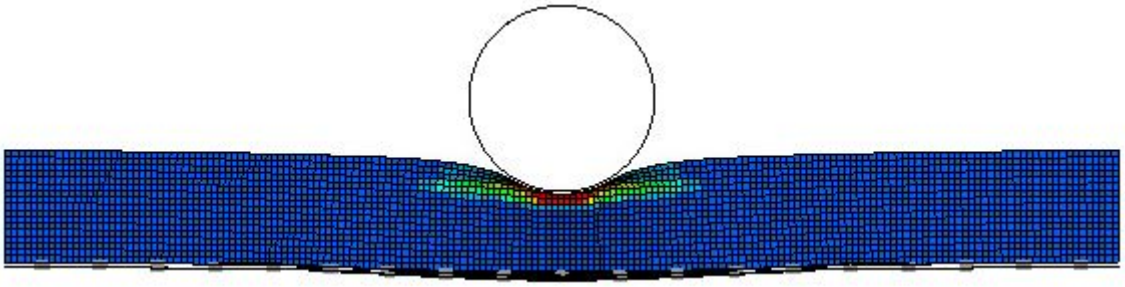

The first element has failed.

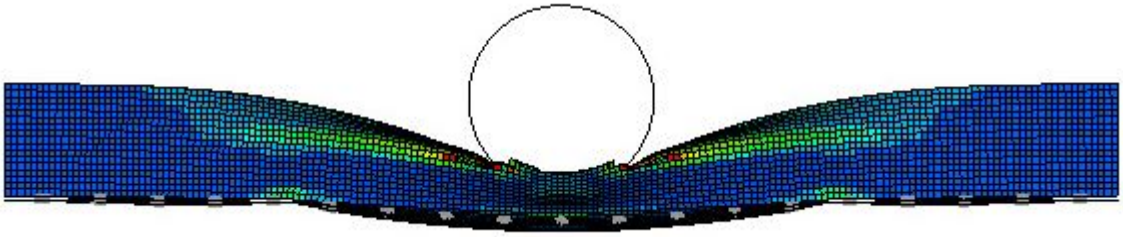

After full loading.

Figure 25: The B-Pillar simulated with CrachFEM as material model. Three different points in time are displayed.

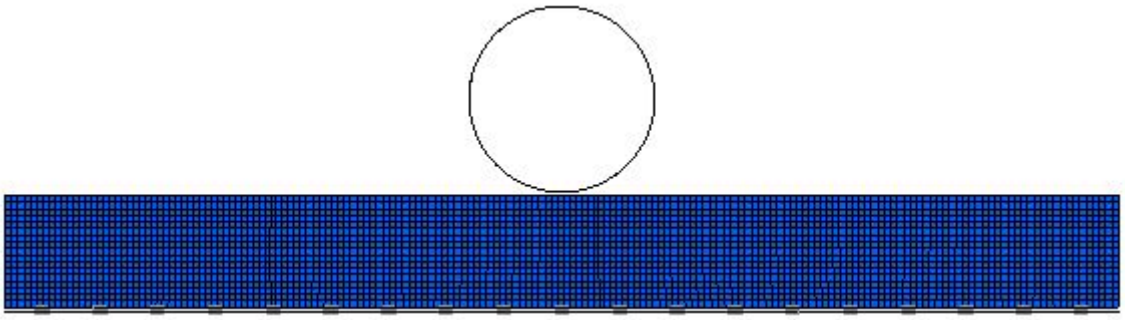

Before loading is applied.

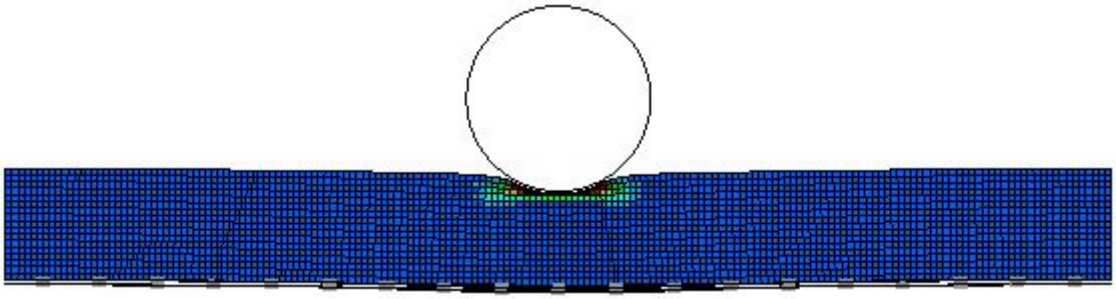

The first element has failed.

After full loading.

Figure 26: The B-Pillar simulated with GISSMO as material model. Three different points in time are displayed.

The results from the B-pillar simulation modelled by the two material models are similar. Since CrachFEM work as a failure criteria, the initiation of failure is the focus. Figure 27 and Figure 28 show the first element that fails for CrachFEM and GISSMO respectively. Since the element that fails first is in the same region and fail within a short period of time for CrachFEM and GISSMO, the GISSMO is considered good enough and will be used for further investigation in the rear crash load case.

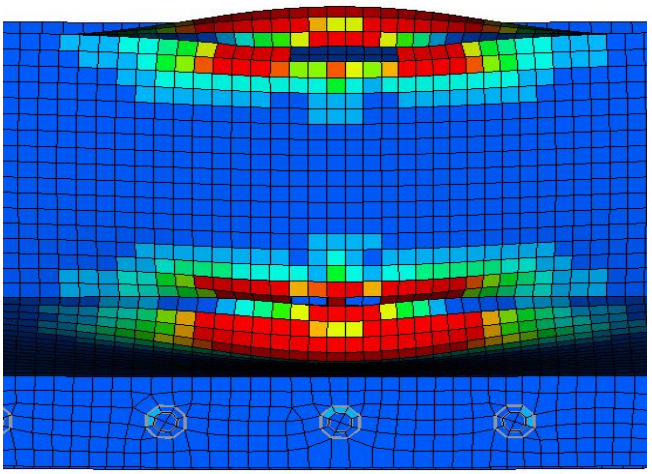

Figure 27: First element failed with CrachFEM. The B-pillar is here seen from above.

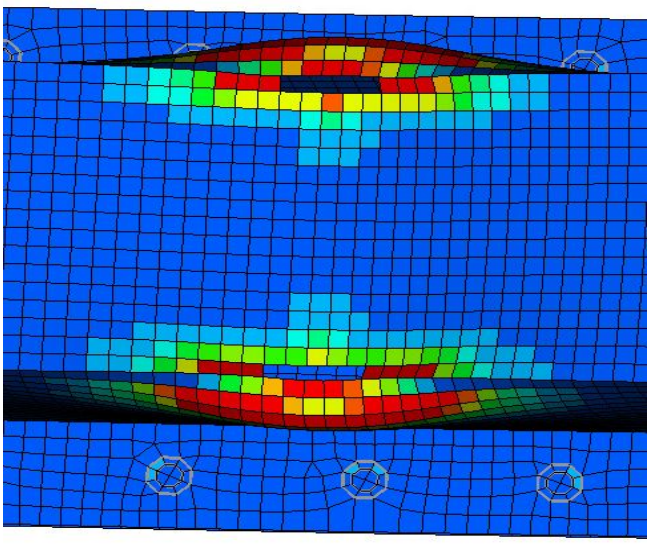

Figure 28: First element failed with GISSMO. The B-pillar is here seen from above.

The time has been an key factor for this thesis. For the result to be valid it is important that the same CPUs are chosen in the cluster. This is important since different CPUs can have different quality. The B-pillar simulation took 3 hours, 22 minutes and 56 seconds when running with MF GenYld+CrachFEM and 51 minutes and 52 seconds with *MAT_024 and GISSMO. See Figure 29 and 30 for detailed information about the run time. The "Contact algorithm" and "Rigid bodies" calculations are specific calculations for the B-Pillar simulation and do not depend on which material model that is used. Hence, to get a fair comparison of the time reduction, the "Element processing" stage should be considered instead of "Total CPU time". The "Element processing" takes 180 min 39 s with CrachFEM and 31 min 49.9s with GISSMO. GISSMO results in a time reduction of the "Element processing" of almost 82 percent compared to CrachFEM. Thereby, GISSMO has a huge potential of reducing the simulation time, especially when a full car body simulation normally takes about 14 hours modelled with CrachFEM.

```
T i m i n g   i n f o r m a t i o n
                          CPU(seconds)   %CPU  Clock(seconds) %Clock
 ------------------------------------------------------------------
 Initialization ....... 6.4827E+00    0.05     7.0341E+00    0.06
 Element processing ... 1.0829E+04   88.88     1.0839E+04   88.87
 Binary databases ..... 1.6029E+00    0.01     1.6947E+00    0.01
 ASCII database ....... 5.1009E-01    0.00     6.3705E-01    0.01
 Contact algorithm .... 1.3001E+03   10.67     1.3010E+03   10.67
   Interf. ID        1 3.1581E+02    2.59     3.1596E+02    2.59
   Interf. ID        2 9.3489E+02    7.67     9.3542E+02    7.67
 Contact entities ..... 0.0000E+00    0.00     0.0000E+00    0.00
 Rigid bodies ......... 4.6760E+01    0.38     4.6651E+01    0.38
 Implicit Nonlinear ... 0.0000E+00    0.00     0.0000E+00    0.00
 Implicit Lin. Alg. ... 0.0000E+00    0.00     0.0000E+00    0.00
 ------------------------------------------------------------------
 T o t a l s           1.2184E+04  100.00     1.2196E+04  100.00

Problem time       =    5.0000E+01
Problem cycle      =    265543
Total CPU time     =     12176 seconds (   3 hours 22 minutes 56 seconds)
CPU time per zone cycle  =      1719 nanoseconds
Clock time per zone cycle=      1721 nanoseconds

Parallel execution with      2 MPP proc
NLQ used/max               120/   120
```

Figure 29: Timing information MY GenYld+CrachFEM, B-pillar.

```
T i m i n g   i n f o r m a t i o n
                          CPU(seconds)   %CPU  Clock(seconds) %Clock
 ------------------------------------------------------------------
 Initialization ....... 6.6436E+00    0.21     8.2172E+00    0.26
 Element processing ... 1.9086E+03   61.24     1.9099E+03   61.20
 Binary databases ..... 1.6205E+00    0.05     1.8677E+00    0.06
 ASCII database ....... 3.6417E-01    0.01     6.0807E-01    0.02
 Contact algorithm .... 1.1594E+03   37.20     1.1602E+03   37.18
   Interf. ID         1 2.5903E+02    8.31     2.5913E+02    8.30
   Interf. ID         2 8.5239E+02   27.35     8.5283E+02   27.33
 Contact entities ..... 0.0000E+00    0.00     0.0000E+00    0.00
 Rigid bodies ......... 4.0135E+01    1.29     4.0034E+01    1.28
 Implicit Nonlinear ... 0.0000E+00    0.00     0.0000E+00    0.00
 Implicit Lin. Alg. ... 0.0000E+00    0.00     0.0000E+00    0.00
 ------------------------------------------------------------------
 T o t a l s            3.1167E+03  100.00     3.1208E+03  100.00

Problem time       =    5.0000E+01
Problem cycle      =    262448
Total CPU time     =      3112 seconds (   0 hours 51 minutes 52 seconds)
CPU time per zone cycle  =       444 nanoseconds
Clock time per zone cycle=       444 nanoseconds

Parallel execution with      2 MPP proc
NLQ used/max               120/   120
```

Figure 30: Timing information, *MAT_024 and GISSMO, B-pillar.

4.4.2 Rear crash

The final verification of that GISSMO has been implemented correctly is to analyze a complex load case of a car crash where the rear of the car will be hit by a wagon with a defined velocity. Figure 44 in the Appendix visualize the load case. This test will be focused on what happens with the rear bumper during collision. The first simulation will model the bumpers behaviour with CrachFEM and the second will model it with GISSMO.

There is a reason why the simulation time is not the focus during this load case. That is because different parts of the car are modelled with different material models. Some of these models do not model material failure since it is not necessary in all areas and it would extend the simulation time further. During this simulation, it is only the material model of the bumper that is changed between the two simulations.

The results will illustrate only the bumper, to make the analysis more clear. Figure 31 and 32 show the deformation of the bumper, from above, at three different points in time. Figure 31 is modelled by CrachFEM and Figure 32 is modelled by GISSMO. The color of the figures represent the equivalent plastic strain.

Undeformed bumper.

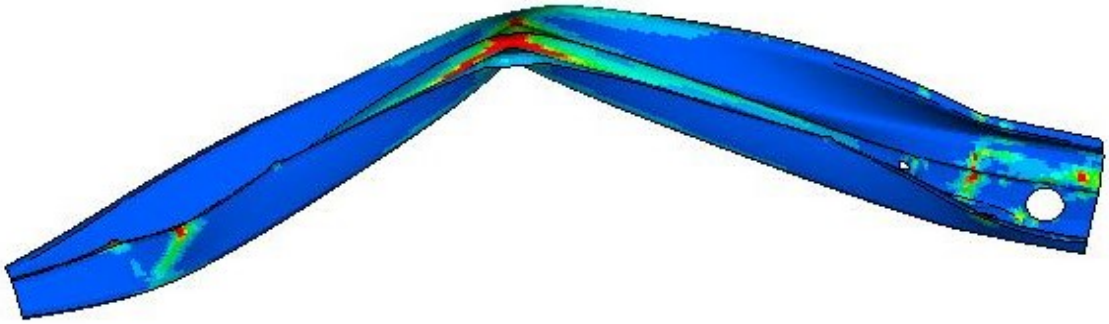

The first element has failed.

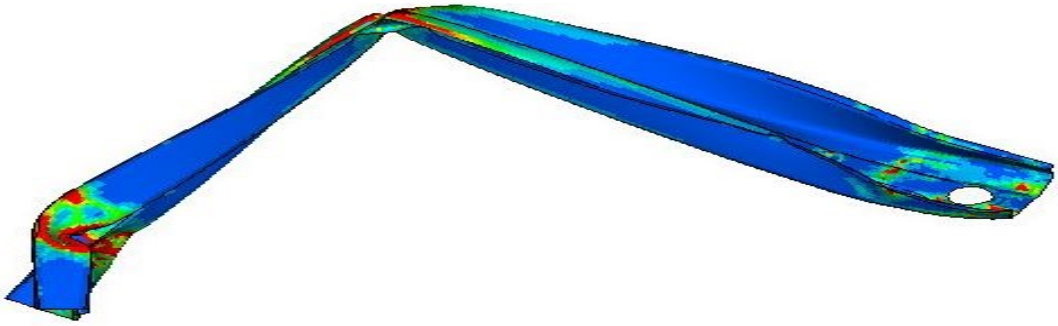

Fully loaded

Figure 31: The deformation of the bumper at three different time steps during loading. Modelled with CrachFEM

Undeformed bumper.

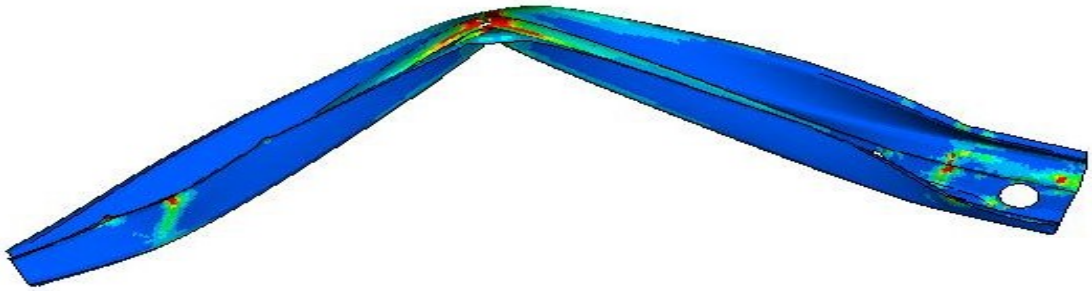

The first element has failed.

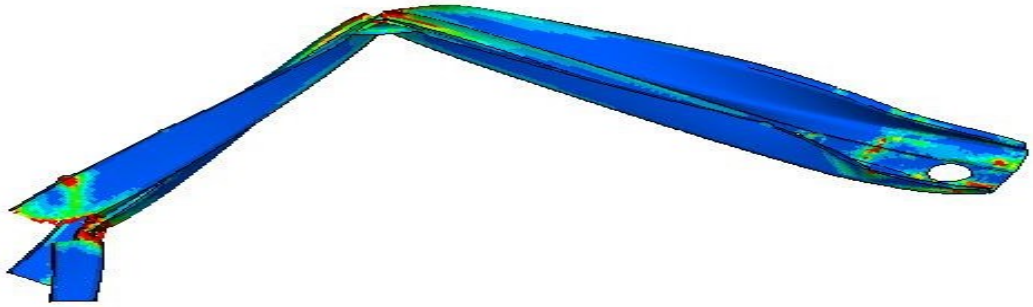

Fully loaded

Figure 32: The deformation of the bumper at three different time steps during loading. Modelled with GISSMO

The deformations look similar, but a more detailed analysis is needed to evaluate the result. Figure 33-36 show the bumper, viewed from behind, in its undeformed geometry to be able to compare the results easier. Figure 33 and 34 show how the location of the failure and equivalent plastic strain is varying when the first element has failed. Figure 35 and 36 show how the location of the failure and equivalent plastic strain is varying after full loading. Overall, the results are similar. It is noticed that

more elements fail using GISSMO than using CrachFEM. Although, the CrachFEM manual [5] claims that CrachFEM should only be used to determine the initiation of material failure, which is very similar between GISSMO and CrachFEM.

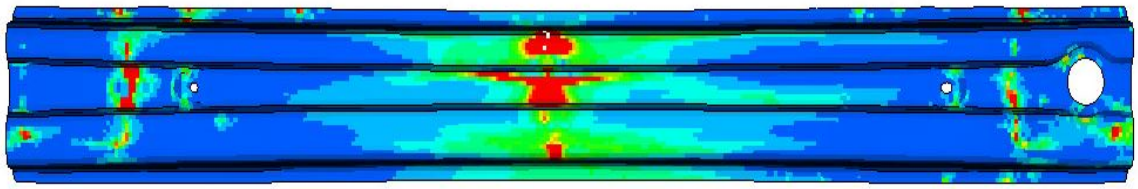

Figure 33: First element failed. Modelled with CrachFEM.

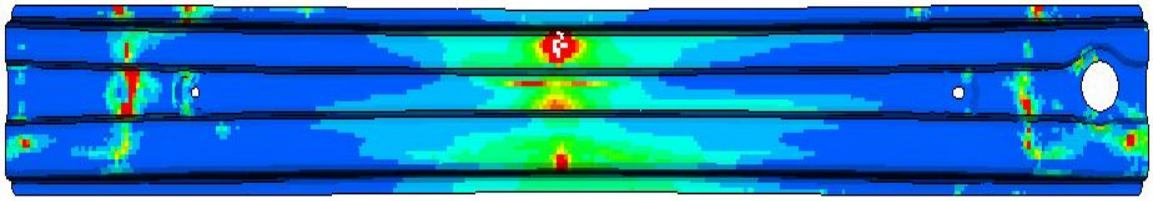

Figure 34: First element failed. Modelled with GISSMO.

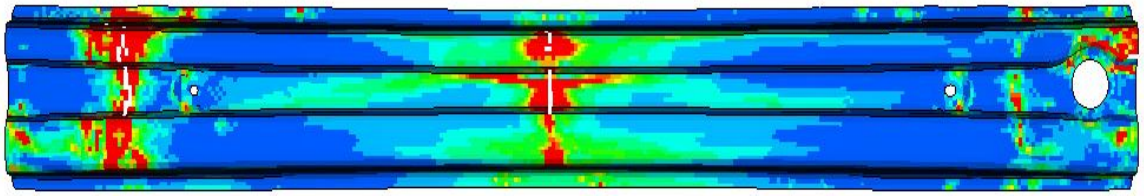

Figure 35: After full loading. Modelled with CrachFEM.

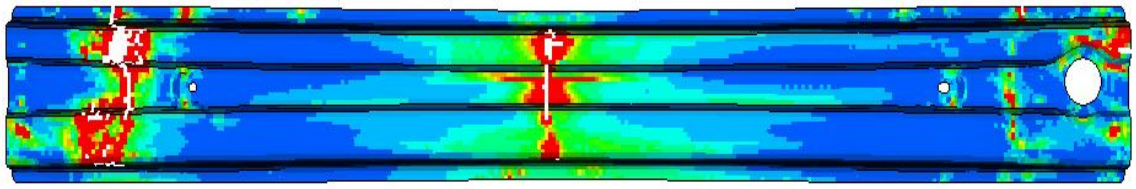

Figure 36: After full loading. Modelled with GISSMO.

5 Analysis

The final comparisons of the material models show similar results. This indicates that the parameter identification process works. However, there are some stages that may be improved. For example, the triaxiality gap between the shear 0° and uniaxial tension test which was previously mentioned, see Figure 9. It may be difficult to design a test specimen that obtains the wanted triaxiality, but since this thesis is not based on experimental test results, the material testing does not need to be limited by standardized test specimens. It is possible to replace the specimens with a load case of one element, see Figure 37. All different triaxialities can be generated with this simple test by changing the displacement controlled loading. This would improve the process in a couple ways. Partly because of reduced simulation time during the material testing and partly because it is possible to direct the stress state in a simple way. This testing method has been tried, and seems to work well. One problem that arose with this testing technique is with a pure shear test with a stress state characterized by $\eta = 0$. Regardless of how long the loading proceeds, the element does not fail. Since the CrachFEM parameters are encrypted, it is difficult to address why this is the case. It is definitely a testing method that could be further developed.

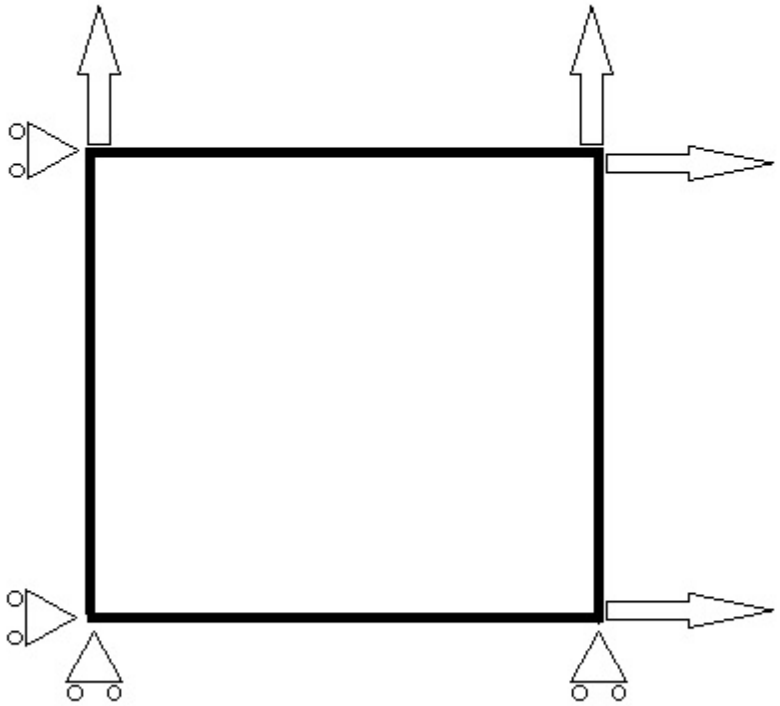

Figure 37: Load case for one element

One potential with GISSMO is to satisfy the problem that Andrade, Feucht and Haufe [1] highlights, which is the information gap between the stages in the process chain and especially between the forming and crash stage. GISSMO is a model which can be used in all product simulations throughout the chain. With GISSMO it is possible to accumulate and transfer variables between these stages. Hence, a more faithful result may be achieved from the crash simulation. This has not been the focus during this thesis, but it is a potential improvement of the material modelling in the automotive industry.

This thesis has developed a method to implement GISSMO based on computer simulations modelled by another material model. One problem that should be flagged for is that there could be some problems by calibrating a material model without access to any experimental material tests. Even though CrachFEM is based on an extensive set of material tests, there could still be deviations between a simulated and an experimental result. The deviations may be extended by the gap between GISSMO and CrachFEM, which could make GISSMO come further away from the reality.

6 Conclusions

*MAT_024 and GISSMO were implemented to analyze the elasto-plastic and the failure behaviour of a material. The material data for the input parameters were generated from computer simulations using MF GenYld+CrachFEM. *MAT_024 and GISSMO were compared with MF GenYld+CrachFEM during two complex load cases, one depicting a B-pillar and one depicting a full car body rear crash. The new material model has proven to have a potential to reduce the simulation time with almost 82 percent and has similar material behaviour as the current model. However, one limitation of the result is that *MAT_024 and GISSMO have not been compared to experimental data.

References

[1] Filipe ANDRADE, Markus FEUCHT, and Andre HAUFE. On the prediction of material failure in ls-dyna®: A comparison between gissmo and diem. In *13th International LS-DYNA® Users Conference*, 2014.

[2] Donald R Askeland and Pradeep Prabhakar Phulé. The science and engineering of materials. 2003.

[3] Percy Williams Bridgman. *Studies in large plastic flow and fracture*, volume 177. McGraw-Hill New York, 1952.

[4] Livermore Software Technology Corporation. Ls-opt user's manual. 2015.

[5] Helmut. Oberhofer Gernot. Dell, Harry. Gese. *MF GenYld+CrachFEM 4.2 User's Manual*. 2014.

[6] Oana CAZACU Dorel BANABIC, Frederic BARLAT, Dan-Sorin COMSA, Stefan WAGNER, and Kurt SIEGERT. Recent anisotropic yield criteria for sheet metals. 2002.

[7] J Effelsberg, A Haufe, M Feucht, F Neukamm, and P Du Bois. On parameter identification for the gissmo damage model. In *12th International LS-DYNA® Users Conference, Dearborn, MI, USA*, 2012.

[8] American Society for Testing and Material. *Standard Test Methods for Tension Testing of Metallic Materials*. 1998.

[9] John O Hallquist et al. Ls-dyna theory manual. *Livermore software Technology corporation*, 3, 2006.

[10] André Haufe, Paul DuBois, Frieder Neukamm, and Markus Feucht. Gissmo–material modeling with a sophisticated failure criteria. In *LS-Dyna Developer Forum*, 2011.

[11] Rodney Hill. A theory of the yielding and plastic flow of anisotropic metals. In *Proceedings of the Royal Society of London A: Mathematical, Physical and Engineering Sciences*. The Royal Society, 1948.

[12] Jean Lemaitre and Jean-Louis Chaboche. *Mechanics of solid materials*. Cambridge university press, 1994.

[13] Livermore Software Technology Corporation (LSTC). *LS-DYNA User's Manual Volume II, Verision R7.0*. 2013.

[14] Frieder Neukamm, Markus Feucht, and André Haufe. Considering damage history in crashworthiness simulations. *Ls-Dyna Anwenderforum*, 2009.

[15] Niels Saabye Ottosen and Matti Ristinmaa. *The mechanics of constitutive modeling*. Elsevier, 2005.

[16] J R_ Rice and Dennis Michael Tracey. On the ductile enlargement of voids in triaxial stress fields. *Journal of the Mechanics and Physics of Solids*, 17(3):201–217, 1969.

[17] BETA CAE Systems SA. Ansa user's guide. 2015.

[18] Katharina Witowski, Markus Feucht, and Nielen Stander. An effective curve matching metric for parameter identification using partial mapping. In *8th European LS-DYNA, Users Conference Strasbourg, pgs*, pages 1–12, 2011.

[19] Liang Xue. Damage accumulation and fracture initiation in uncracked ductile solids subject to triaxial loading. *International Journal of Solids and Structures*, 44(16):5163–5181, 2007.

[20] Won Y Yang, Wenwu Cao, Tae-Sang Chung, and John Morris. *Applied numerical methods using MATLAB*. John Wiley & Sons, 2005.

7 Appendix

7.1 Test specimens

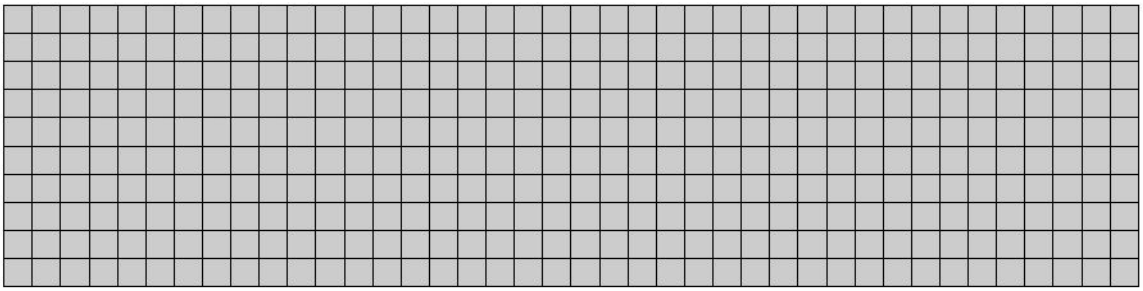

Figure 38: Uniaxial tension test specimen

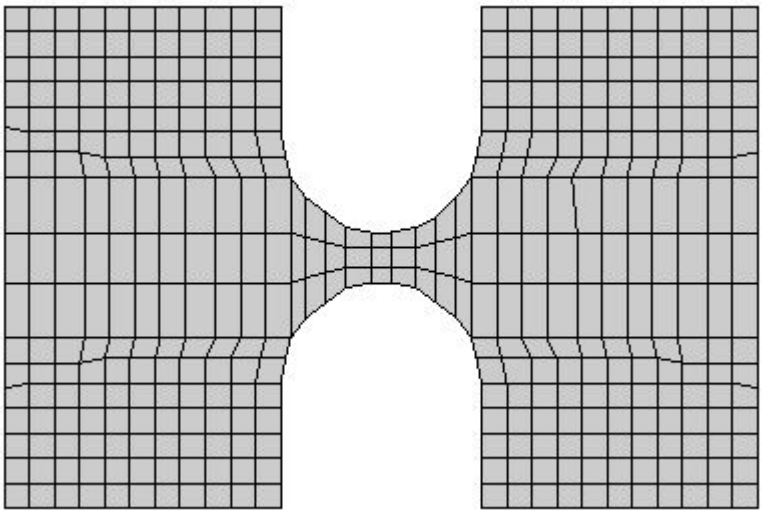

Figure 39: Notch test specimen, radius 4 mm

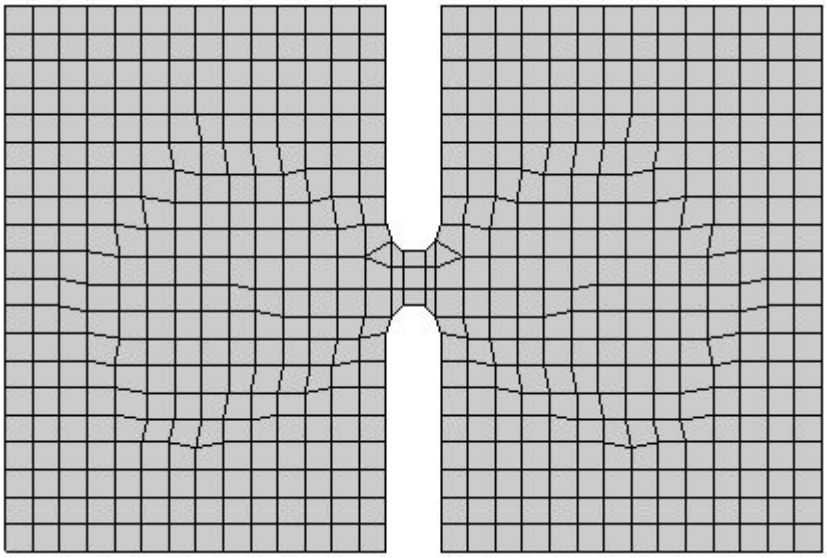

Figure 40: Notch test specimen, radius 1 mm

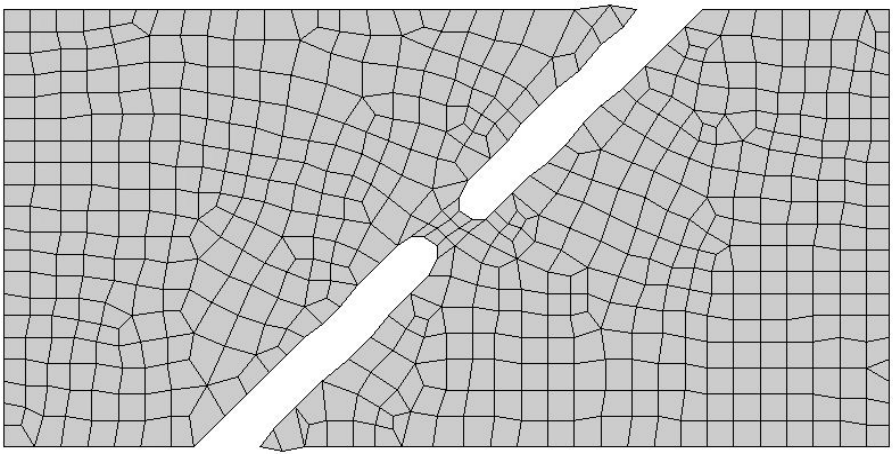

Figure 41: Shear 45° test specimen

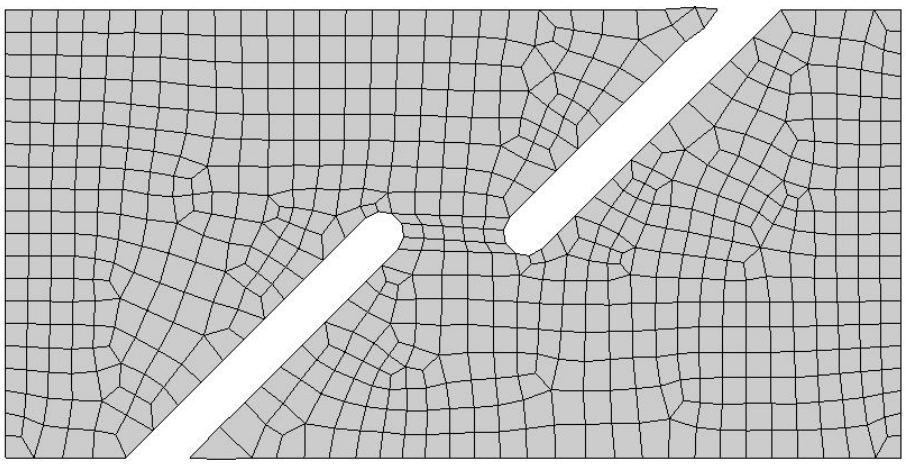

Figure 42: Shear 0° test specimen

7.2 B-Pillar

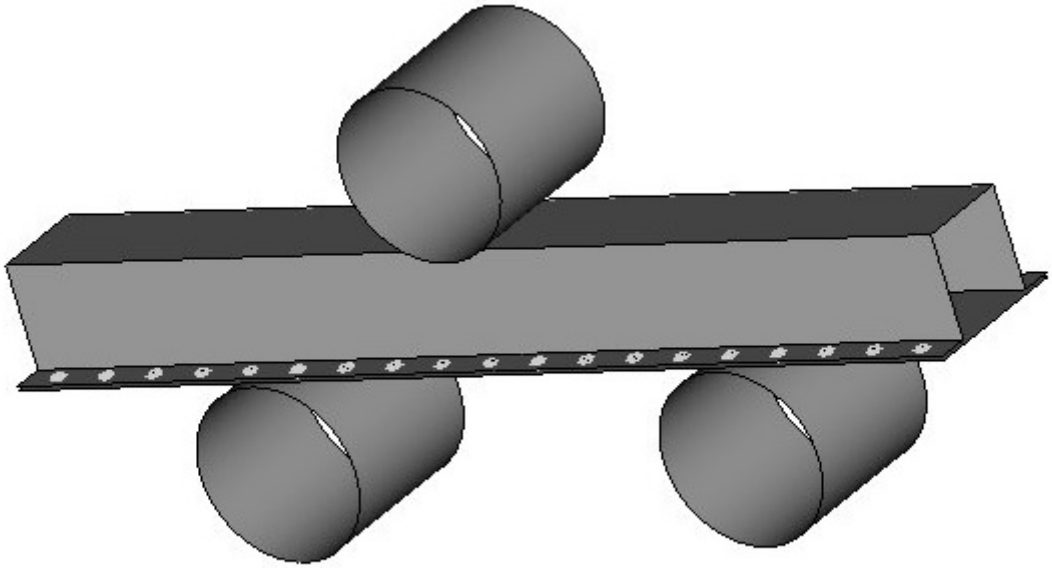

Figure 43: The geometry of the B-pillar.

7.3 Rear crash

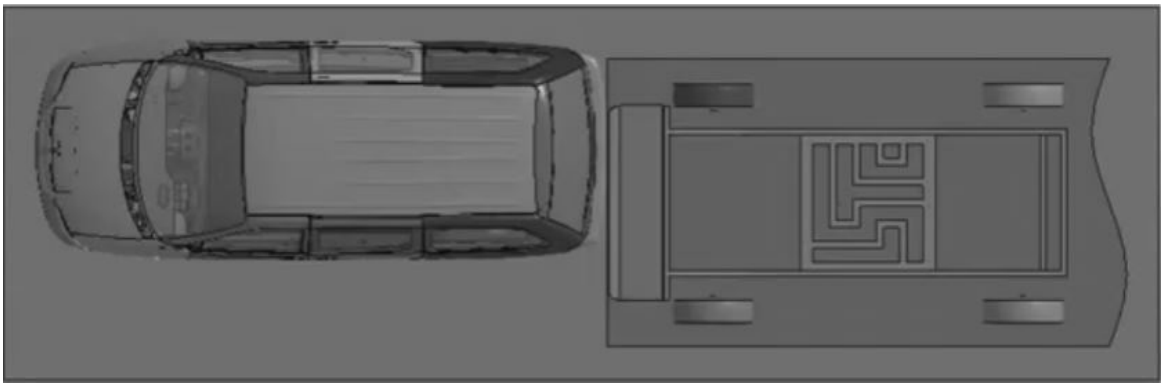

Figure 44: The geometry of a similar rear crash test.